Insights into Bioprinted Smooth Muscle Tissue Models for Treatment of Urethral Strictures

Xuan, Zongzhe

DOI (link to publication from Publisher):
10.54337/aau513984105

Publication date:
2022

Document Version
Publisher's PDF, also known as Version of record

INSIGHTS INTO BIOPRINTED SMOOTH MUSCLE TISSUE MODELS FOR TREATMENT OF URETHRAL STRICTURES

BY
ZONGZHE XUAN

DISSERTATION SUBMITTED 2022

AALBORG UNIVERSITY
DENMARK

INSIGHTS INTO BIOPRINTED SMOOTH MUSCLE TISSUE MODELS FOR TREATMENT OF URETHRAL STRICTURES

PHD DISSERTATION

by

Zongzhe Xuan

AALBORG UNIVERSITY
DENMARK

Regenerative Medicine Group

Dissertation submitted: September 2022

PhD supervisor: Assoc. Prof. Cristian Pablo Pennisi
Regenerative Medicine Group
Department of Health Science and Technology
Aalborg University, Aalborg, Denmark

PhD committee: Associate Professor Maj Schneider Thomsen
Aalborg University, Denmark

Associate Professor Melanie Hart
University of Freiburg Medical Center, Germany

Associate Professor Johan Ulrik Lind
Technical University of Denmark, Denmark

PhD Series: Faculty of Medicine, Aalborg University

Department: Department of Health Science and Technology

ISSN (online): 2246-1302
ISBN (online): 978-87-7573-822-9

Published by:
Aalborg University Press
Kroghstræde 3
DK – 9220 Aalborg Ø
Phone: +45 99407140
aauf@forlag.aau.dk
forlag.aau.dk

Printed in Denmark by Stibo Complete, 2022

TABLE OF CONTENTS

CV

Zongzhe Xuan

Date of birth: 8 October 1988

+45 50146712; zxuan@hst.aau.dk

https://www.linkedin.com/in/zongzhe-xuan-8a4044234

➢ PROFESSIONAL EXPERIENCE

Ph.D., Aalborg University, DK **2018 - 2022**

- Research topic: Development of Biomimetic Grafts for Urethral Reconstruction

Medical Assistant, Patiro, Patient Recruitment, DK **2022**

- Title: Medical Assistant

Medical Doctor, First Hospital of Jilin University, CN **2014 - 2018**

- Title: Thoracic Surgeon

National Resident Standardized Training, **2015 - 2018**

First Hospital of Jilin University, CN

- Title: Surgery Residency (Cardiothoracic Surgery)

➢ EDUCATION

Ph.D., Aalborg University, DK **2018 - 2022**

Master in Surgery, First Hospital of Jilin University, CN **2015 – 2018**

➢ SCIENTIFIC ACTIVITIES

Lectures in Regenerative Medicine, 2nd semester Medis/Medicine **2021 - 2022**
Aalborg University, DK

Project supervision on 4th semester Medis and 2 guest master students **2021 - 2022**

Poster presentation: 1st Annual Biomedicine Meeting, Aalborg **2021**

Poster + Oral presentation: 6th World Congress of the Tissue Engineering **2021**
and Regenerative Medicine International Society, Maastricht, NL

Study abroad: Polymer Chemistry & Biomaterials Group **2020**
Centre of Macromolecular Chemistry, Ghent University, BE

➢ GRANTS

S.C. Van Fonden: 75,000 DKK **2021**

Short Term Scientific Mission (COST): 1100 EUR **2020**

- European Cooperation in Science and Technology

State Scholarship Fund: 252,000 DKK **2019**

- China Scholarship Council

➢ PUBLICATIONS IN JOURNALS

- Peng, Q., **Xuan, Z.,** Pennisi, P., Porsborg, S. R., Fink, T. & Zachar, V. (2022). Distinct dominant lineage from in vitro expanded adipose-derived stem cells (ASCs) exhibits enhanced wound healing properties. Cells, 11(7), 1236.
- Peng, Q., **Xuan, Z.**, Pennisi, P., Porsborg, S. R., Fink, T. & Zachar, V. (2021). Multiplex Analysis of Adipose-Derived Stem Cell (ASC) Immunophenotype Adaption to In Vitro Expansion. Cells, 10(2), 218.
- **Xuan, Z**., Cai, H., Chen, C., & Cui, Y. (2018). Effects of silencing p27RF-Rho expression on the biological behavior of A549 human non-small cell lung cancer cells. Int J Clin Exp Med, 11(5),4752-4761.
- **Xuan, Z**., Zachar, V. & Pennisi, P. Source, Selection, and differentiation of cell for tissue engineering and regeneration of the urethra. *Submitted.*
- **Xuan, Z.**, Peng, Q., Larson, T., Christiansen, JDC., Zachar, V. & Pennisi, P. Tailoring hydrogel composition and stiffness to control smooth muscle cell differentiation in bioprinted constructs. *Submitted.*
- **Xuan, Z.**, Gurevich, L., Zachar, V. & Pennisi, P Bioprinted bladder smooth muscle constructs exposed to cyclic mechanical stimulation show enhanced contractile phenotype through p38 activation. *Manuscript in preparation*

➢ CONFERENCE ABSTRACTS

- **Xuan, Z**., Pitsa, A., Zachar, V. & Pennisi, P. "Bioprinting of Smooth Muscle Constructs for Urethral Tissue Engineering" joint TERMIS European Chapter Meeting. May 2020, Manchester, UK.
- **Xuan, Z.,** Damme, L.V., Vlierberghe, S.V., Zachar, V.& Pennisi, P. "Tailoring the properties of gelatin methacrylate (GelMA)/alginate hydrogel blends for bioprinting of smooth muscle constructs" joint 6th World Congress of the Tissue Engineering and Regenerative Medicine International Society. Nov 2021, Maastricht, NL.

ACKNOWLEDGEMENTS

Now, it is raining autumn outside the window, which was also the season when I first arrived in Denmark. In the blink of an eye, four years have passed. With tens of thousands of words coming to an end, I want to save the last inspiration for the chapter of acknowledgements.

First of all, I would like to express my most sincere thanks to my supervisor, Associate Professor Cristian Pablo Pennisi, whose humility and respect I have felt since my first day in the regenerative medicine group. For the past four years, he has been providing me with helpful guidance and valuable advice in the professional field. He also always helped me build confidence when I was in trouble. Over the years, he encouraged almost all of my ideas and allowed me to work with a high degree of freedom. And he was always understanding and considerate when I had any non-work-related issues. I thank God for the opportunity to continue working with him in this way.

In addition to my supervisor, I also benefited from other professors in the regenerative medicine group. While we don't always meet, I know they're there when I need help. Because they've been doing it for the past four years. I would also like to express my heartfelt thanks to Professor Jesper and Leonid for their professional and patient help with my project in the fields of materials and mechanics.

I would like to say thank you to my colleagues in the office who are with me every day. They were the people who really worked side by side with me during my Ph.D. No matter how sad or happy I am, I can feel the warmth in their hearts. For three of the four years I was a PhD student, unable to go home due to Covid-19, I would like to pay tribute to the great friends I made in Aalborg who have always made me feel like we are one family here too.

Also, a special thanks to my brother and best friend, Lei, who opened the door for me from China to Denmark. For the past four years, he has been like family, taking care of me and caring about me. He would push me when I get carried away. He was the guiding light in my life when I was lost.

Thanks to my parents for showing me the way forward and ensuring my growth. Thanks to my strict father for keeping me following a rule, and to my loving mother for keeping me a comfortable life. Thanks to my elderly paternal grandmother and maternal grandmother who have always missed me and maintained this sense of pride even though they didn't know much about my research. I guess I'm just standing on their shoulders and seeing a world they haven't seen, and I'm going to tell them what I've seen.

Thanks to my lover, Geng, she has accompanied me through thick and thin every day for the past four years; the four years of study time not only made us better on the road of life, but also made us more understanding, tolerant and caring for each other. Thanks also to my two cats, they watch over me when they're quiet and always make me happy when they're naughty.

Finally, I would like to thank myself and the experience of the past four years. Thanks for taking the time to not only become a Ph.D., but a more peaceful, compassionate, and stronger person.

While the doctoral dissertation is over, there is still a long way to go in an academic career. "Learning is the sweet fruit from the bitter root". No matter how difficult the process is, I will believe and look forward to that sweetness.

ABSTRACT

Three-dimensional (3D) bioprinting is emerging as a powerful tool for the development of new therapies by enabling the fabrication of tissues that mimic the complex native organization. The aim of this PhD thesis was to develop an in vitro model of urethral smooth muscle using a novel 3D bioprinting approach to study the effects of mechanical signals on smooth muscle phenotype.

Initially, a literature review was conducted to investigate the cell source and approach for the model. The experimental model was based on human bladder smooth muscle cells (SMCs) suspended in hydrogels comprising gelatin methacrylate (GelMA) and alginate.

In Study I, an optimal hydrogel combination was found, which resulted in better structural stability after crosslinking and exhibited high survival, morphology, and proliferation of the SMCs. Interestingly, the results revealed that the stiffness of the 3D construct was critical for maintaining the contractile SMC phenotype.

In Study II, a custom modification of commercially available cell-stretching plates allowed the application of cyclic mechanical stimulation to 3D constructs. The study demonstrated that cyclic mechanical strain significantly enhanced SMC differentiation of cells grown on the constructs, and this effect was mediated by activation of p38 MAPK.

Overall, the results of this work contribute to a better understanding of how mechanical signals from the microenvironment are critical for maintaining the contractile phenotype of SMCs. Hydrogel combinations that exhibit optimal printability, while supporting proper assembly and maturation of the SMCs, may be significant for the development of future treatments for urethral strictures.

DANSK RESUMÉ

Tredimensionel (3D) bioprint har udviklet sig hurtigt som et vigtigt værktøj der giver mulighed for fremstilling af cellemodeller, der efterligner den komplekse arkitektur og sammensætning af levende væv. Formålet med denne Ph.d.-afhandling var at udvikle en *in vitro*-model af urinrørets glatte muskulatur ved hjælp af en 3D bioprinting proces til at undersøge virkningerne af mekaniske signaler på fænotypen af glat muskulatur.

Indledningsvis blev der gennemført en litteraturgennemgang for at undersøge forskellige celletyper og tilgange til modellen. Den eksperimentelle model var baseret på glatte muskelceller fra human blære (SMC) fordelt i et gelbaseret materiale der indeholdte gelatin-methacrylat (GelMA) og alginat.

I undersøgelse 1 blev en optimal gel kombination fundet, hvilket resulterede i bedre mekanisk stabilitet og samtidig viste høj overlevelse, spredning, og vækst af SMC. Derudover, afslørede resultaterne, at stivheden af 3D-modellen var kritisk for at opretholde den kontraktile fænotype af SMC.

I undersøgelse 2 tillod en tilpasset modifikation af cellestrækplader anvendelsen af cyklisk mekanisk stimulering til 3D- modellerne. Undersøgelsen viste, at cyklisk mekanisk stræk forbedrede differentiering af SMC markant, og at denne effekt blev medieret af aktivering af p38 MAPK.

Samlet set bidrager resultaterne af dette arbejde til en bedre forståelse af, hvordan mekaniske signaler fra mikromiljøet er afgørende for at opretholde den kontraktile fænotype af SMC. Gel-kombinationer, der udviser optimal printbarhed, samtidig med at de understøtter korrekt samling og modning af SMC, kan være væsentlige for udviklingen af fremtidige behandlinger for urinrøretsforsnævringer.

LIST OF ABBREVIATIONS

ASCs	Adipose-derived stem cells
α-SMA	Smooth muscle alpha actin
BMP4	Bone morphogenetic protein 4
cDNA	Complementary DNA
CTS	Cyclic tensile strain
DM	Differentiation medium
ECM	Extracellular matrix
EGF	Epidermal growth factor
FBS	Fetal bovine serum
FGF-b	Fibroblast growth factor-basic
GelMA	Gelatin methacrylate
GM	Growth medium
MHC	Smooth muscle myosin heavy chain
PBS	Phosphate buffered saline
PDMS	Polydimethylsiloxane
qRT-PCR	Real time reverse transcription polymerase chain reaction
RFU	Relative fluorescence units
SD	Standard deviation
SMCs	Smooth muscle cells
TE	Tissue engineering
TGF-β1	Transforming growth factor-β1
2D	Two-dimensional
3D	Three-dimensional

CHAPTER 1. INTRODUCTION

Because of its anatomical structure, the male urethra is susceptible to a variety of disorders, including traumatic and acquired injuries. As a consequence of such injuries, urethral strictures may occur, which are characterized by progressive formation of scar tissue in the urethral lumen. Urethral narrowing can cause a number of clinical symptoms that severely affect patients' health and reduce their quality of life[1]. The main surgical approach to repair severe urethral strictures is surgical intervention using a graft, also known as urethroplasty [2]. Surgeons use a variety of tissues for urethroplasty, including oral mucosa and skin. However, the use of these tissues is often limited by complications during harvesting and the limited availability of material to meet clinical needs [3].

Tissue engineering (TE) principles provide an ideal solution for restoring and maintaining normal tissue and organ function by combining elements of biology, materials science, medicine, and engineering[4]. Over the past two decades, various tissue engineered urethral models have been developed to address the problems associated with conventional urethral grafts[5]. Creating a tissue-engineered urethra that mimics the complex tissue functional structure of the natural urethra by using porous polymeric biomaterials as scaffolds and living cells represents an important challenge[6]. Although relevant studies have been confirmed in preclinical models, clinical trials have had limited success. Failure of tissue engineered grafts is mainly due to inadequate blood supply and impaired nutrient exchange after scaffold insertion, as well as defects in the cellular phenotype of urethral tissue[7]. For example, smooth muscle cells do not differentiate into a contractile phenotype, which are essential for maintaining urethral strength and contractile response[8].

As an alternative to conventional porous scaffolds, hydrogels are considered one of the most promising materials for tissue engineering. Not only do they provide mechanical support for cells by mimicking the natural extracellular matrix, but their high-water content also provides an ideal environment for cell survival [9]. In addition, hydrogels enable the layer-by-layer fabrication of three-dimensional scaffolds (by e.g., 3D bioprinting) to specifically customize scaffold structure and morphology and achieve uniform cell distribution[10]. However, the optimal conditions for proper cell maturation and deposition of the extracellular matrix remain unknown, which may be critical for the mechanical stability of the graft to prevent recurrence of the stricture. In addition, previous studies did not consider that the urethra is constantly exposed to mechanical forces during urination, which play an important role in the differentiation and tissue maturation of the smooth muscle layer.

Therefore, the research in this project aims to develop an innovative *in vitro* model to investigate the structural, mechanical, and molecular signals that are critical for proper cell assembly and differentiation, to ultimately significantly improve the performance of tissue engineered urethral grafts.

CHAPTER 2. BACKGROUND

2.1. Urethral stricture

The male urethra is the conduit that carries urine from the bladder to the outside and acts as an outlet for sperm and glandular secretions during ejaculation[11]. After trauma, infection, congenital disease, or injury to the urethra, fibrous scar tissue forms in the urethra, gradually narrowing the lumen, a condition known as urethral stricture. The incidence of urethral stricture has remained at historically high levels over the last few decades. The overall prevalence of urethral stricture disease in men is 0.6% and men over the age of 65 are more likely to be affected [12]. As the condition progresses, urethral strictures can cause a range of symptoms: straining to pass urine, pain during urination, urinary tract infections and prostatitis. Some patients with severe urethral strictures are even unable to urinate at all and require urgent treatment. As urethral stricture greatly impairs the health and quality of life of patients, there is a growing interest in the medical community to find suitable management options.

Currently, endoscopic treatment by direct visual urethrotomy (DVIU), seems to be gradually becoming the first choice for patients due to its advantages of being minimally invasive and easy to perform [13]. However, it has a low long-term treatment success rate (0-9%) and its scope is limited to single strictures that are less than 2 cm long [14]. In contrast, surgical removal of the affected tissue and reconstruction of the urethra with grafts, urethroplasty, has a much higher long-term success rate (85-90%) and is now considered the gold standard for the treatment of urethral stricture [15]. (Figure 1).

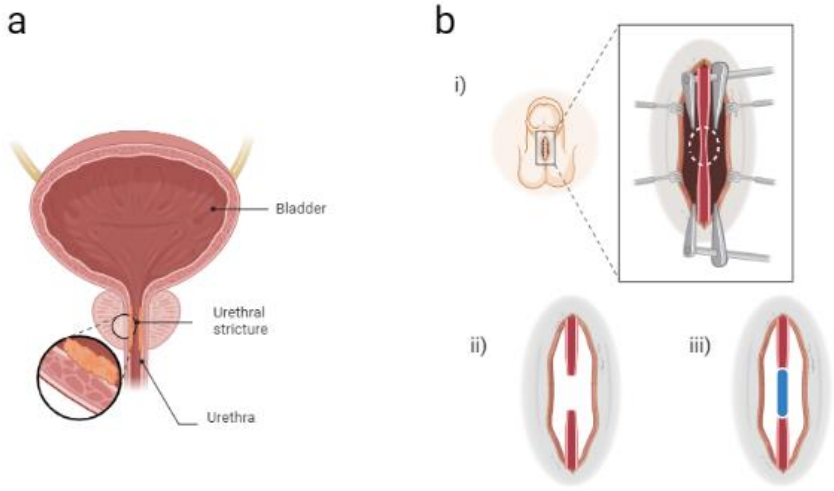

Figure 1. (a) Stricture disease is caused by a narrowing of the urethral lumen at any location between the bladder and the urinary meatus (b) Example of augmentation urethroplasty using a tissue graft for treatment of a distal stricture. The urethral stricture is exposed (i), the damaged tissue is removed (ii), and graft is sutured in place (iii). Figure created with BioRender.com

Two types of grafts are clinically available for urethral reconstruction: skin grafts and oral mucosal grafts. Penile skin was the first graft used for urethral reconstruction [16], but because it tends to form hair in the new urethra, it can lead to urethral calculi, urinary tract infections and hair blockage of the lumen, resulting in restricted urinary flow. Also, due to the poor response of penile skin to the moist environment of the urethra and the low long-term success rate (50%) [17], it is gradually being replaced by oral mucosa grafts. In contrast, oral mucosa has several desirable properties that make it particularly suitable for urethral reconstruction. Firstly, it has good mechanical strength for the procedure. Secondly, it adapts well to the moist environment of the urethra. Finally, it has more favorable vascular properties, giving it a high capacity for rapid absorption of the blood supply to the wound. All these properties give it a lasting success rate of up to 80-85%. For this reason, oral tissue grafts obtained from the oral mucosa (buccal mucosa) are currently considered the gold standard[18].

However, the clinical use of oral mucosa also faces several limitations. Only a limited amount of donor tissue can be collected, and some patients with lesions in the oral mucosa (e.g., oral lichen planus) are unable to have oral mucosa collected to meet the needs of the procedure. In addition, donor site bleeding may occur when collecting buccal mucosa, and complications such as donor site infection, pain, parotid duct damage, graft contracture and numbness may occur after collection [19]. To overcome these difficulties, alternative methods of urethral reconstruction need to be explored.

2.2. The urethral smooth muscle

The muscular layer of the urethra, which performs crucial physiological and structural duties, is crucial to the restoration of the urethral structure and function [20]. At the bladder outlet, an outer layer of striated muscle and an inner layer of smooth muscle form the sphincters that control urine emptying. Along the remaining length of the urethra, there are essentially two layers of smooth muscle cells: a longitudinally oriented inner layer and a circularly oriented outer layer. When urinating, the longitudinal layer contracts, shortening the urethra, while during the filling phase, the circular smooth muscle layer contracts, effectively shortening the urethra. In addition to the nervous system controlling these mechanical actions of the urethral smooth muscle[21], the ECM that covers the smooth muscle layer also aids in preserving the mechanical condition of the urethra. Elastin, for instance, is crucial for urethral compliance due to its high degree of extensibility, whereas collagen gives the urethra the mechanical strength it needs to maintain appropriate physiological structure [22].

2.3. Characterization of smooth muscle cells (SMCs)

SMCs exhibit phenotypic plasticity in that they can transition from a synthetic to a contractile phenotype and vice versa. This phenotype switch is characterized by the expression of a number of smooth muscle (SM)-specific contractile-related proteins[23], including SM-myosin heavy chain (MYH11), SM-α-actin (ACTA2), smooth muscle 22 α (SM22α), transgelin (TAGLN), calmodulin (CNN1), h-caldesmon (CALD1), smoothelin (SMTN), leiomodin 1 (LMOD1), potassium calcium-activated channel subfamily M regulatory beta subunit 1 (KCNMB1), Kv1.5 (KCNA5), and the intermediate filament protein synemin (SYNM). Synthetic SMCs have a hill and valley morphology compared to elongated spindle-shaped morphology that is characteristic of contractile SMCs (Figure 2). Furthermore, synthetic SMCs exhibit higher proliferation, migration, and ECM synthesis rates compared with the contractile SMC phenotype Moreover, the expression of contractile-related proteins are significantly decreased in synthetic SMCs and replaced by non-contractile functional proteins such as β-SMA and MHC10. Signaling molecules such as transforming growth factor beta 1 (TGF-1) or heparin are critical in this phenotypic plasticity. For example, in vascular SMCs, TGF-1 transcriptionally regulates the expression of many genes, resulting in a phenotypic change of the cells toward a contractile phenotype. At the same time, cell-to-cell interactions as well as changes in the stiffness of the extracellular matrix can cause phenotypic switch [24]. (Figure 2)

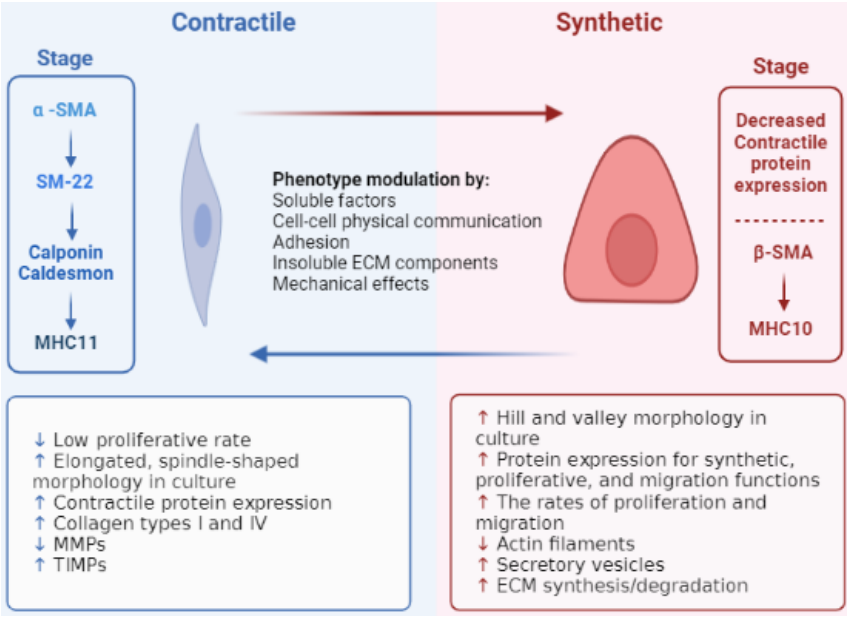

Figure 2. Summary of the characteristics of the VSMC phenotype along the phenotypic continuum between the contractile, differentiated phenotype on the left and the synthetic, de-differentiated phenotype on the right, as well as some environmental cues that affect this continuum and markers for various differentiation processes. Figure created with BioRender.com

2.4. Urethral tissue engineering

As previously mentioned, traditional grafting methods for urethral reconstruction surgery can lead to varying degrees of donor site morbidity and a range of complications. Tissue engineering offers the possibility of replacing and restoring damaged tissue structure and function by combining relevant principles and techniques from materials science, cell biology, transplantation, and engineering [25]. Tissue engineering approaches usually consist of four key steps, including (1) the selection of biomaterials capable of acting as scaffolds with biochemical and mechanical properties suitable for specific clinical applications; (2) the selection of cell sources for seeding on selected scaffolds; (3) biomanufacturing techniques combining biomaterial scaffolds and cells; and (4) environmental parameters, adding bioactive factors to the construct or placing it in dynamic culture mode to achieve the desired results [26]. (Figure 3)

Over the past two decades, various tissue engineering models for urethral regeneration have been developed [5]. For long and complex strictures, the typical approach consists in the use of cell-laden tissue constructs which comprise a porous polymeric biomaterial (scaffold) onto which cells are cultured before implantation.

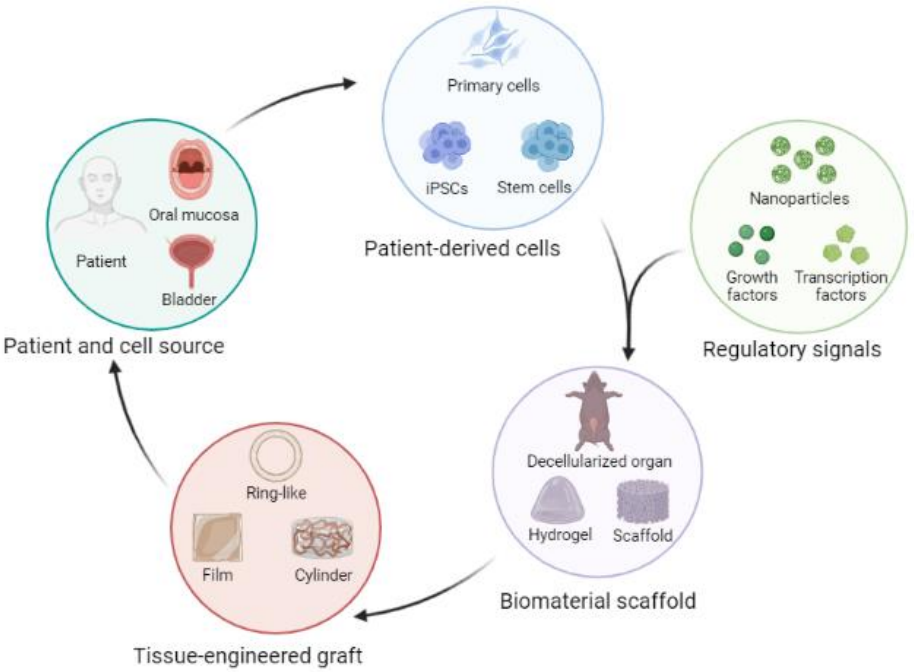

Figure 3. The general path of tissue engineering relevant to the urethra. Patients' cells are removed and grown in cell culture. After being grown, the cells are seeded onto a scaffold that serves as a template and promotes tissue growth and maturation. Once it has fully developed, the tissue can be transplanted into the patient to recover tissue function. Figure created with BioRender.com

2.4.1. Biomaterial scaffolds for urethral TE

Typically, scaffolds for urethral tissue engineering are fabricated with synthetic and/or natural polymers. In general, natural polymers are highly biocompatible but have poor mechanical properties [27,28]. In contrast, synthetic polymers, formed by adjusting their chemical structure and molecular composition, usually exhibit highly tunable biodegradability, biocompatibility, and mechanical properties [29,30]. Table I summarizes the polymeric materials that have been used in tissue engineering of the urethra, most of which have been covered in literature reviews [31,32].

Table I. Polymers used as scaffolds for urethral tissue engineering.

Natural polymers	Synthetic polymers
Collagen[33–37]	PLCL [38]
Gelatin [39,40]	PLLA [41]
Silk fibroin [42–47]	PCL/PLLA [48]
Alginate [49]	PLLA/PEG [50]
Hyaluronic acid/collagen [51]	PCL/PLCL [10]
Cellulose [52]	PLLA/Gelatin [53]
Fibrin [54]	PLCL/Collagen [55]
Chitosan/collagen [56]	PLA [57]
	PU/mesh in PGA [58]
	PLGA [59]
	PLGA/Gelatin [60]
	P-HEMA [61]

Abbreviations: PLCL: poly(l-lactide-co-ε-caprolactone); PCL: poly ε-caprolactone PLA: polylactic acid; PU: polyurethane; PGA: polyglycolic acid; PLGA: poly(lactic-co-glycolic) acid; PLLA: poly-l-lactic acid, P-HEMA: poly(2-hydroxyethyl methacrylate).

The conventional porous scaffold-based approach has a number of limitations. Firstly, the pore sizes formed by different biomaterials do not allow for the exchange of oxygen and nutrients; secondly, some scaffolds constructed from biomaterials have far from optimal mechanical properties and structural and morphological control [62]; and finally, there is still no consensus on the functional cell seeding that facilitates urethral regeneration. These limitations may result in heterogeneous cell growth within the scaffolds, which is thought to be responsible for tissue graft failure and lead to scarring and recurrence of stricture [63].

Hydrogels are three dimensional networks of hydrophilic polymers. They can be cross-linked by physical or chemical means to form gels that swell rapidly in water but can retain large amounts of water in the swollen state without dissolving [61]. Their high-water content facilitates cell encapsulation and allows sufficient transport of nutrients and metabolites to ensure cell viability. Furthermore, by varying the concentration or composition of the hydrogel, not only can the pore size be adjusted to improve cell adhesion and cell proliferation [64], but also physical properties such as degradability and mechanics, providing mechanical support for cells in engineered tissues and mimicking the natural extracellular matrix [65].

In the development of hydrogel scaffolds, researchers have proposed a variety of biomaterials and manufacturing techniques. However, the application of hydrogels as functional scaffolds for tissue engineering still poses many challenges. The pores of the conventional hydrogel mesh may be different from the actual pores of the ECM, which makes it difficult to promote cell proliferation and further differentiation [66].Natural hydrogels possess the biological properties required to promote cellular responses, but their low modulus and poor mechanical properties make it difficult to fabricate stable structures and complex geometric scaffolds. In contrast, synthetic hydrogels generally possess high mechanical strength and easily customizable mechanical and chemical properties, but they lack biologically active molecules that can promote cell adhesion and migration. Therefore, to develop effective hydrogel-based scaffolds for urethral tissue engineering, both their physicochemical and biological properties must be considered and rationally designed.

2.4.2. Cell sources used for urethral TE

In urethral TE, there are two approaches: the first strategy is to rely exclusively on cell-free scaffolds, using natural or synthetic materials. The scaffold is mainly infiltrated by host cells, which remodel the scaffold over time, ideally to be replaced by the target tissue [67]. The benefits of this approach are that it is simple, requires less preoperative preparation and entails fewer procedures [6]. A healthy urethral bed, the absence of spongy fibrosis and adequate vascularity are necessary for the success of a cell-free graft [5]. However, as the underlying pathological process in stricture disease is ischemic fibrosis, the quality of the wound bed may be reduced [68]. Furthermore, this straightforward approach can only be used as a back-up option in patients with small to moderate urethral anomalies, and clinical data suggest that failure is common in people with strictures greater than 4 cm [69].

Cell-based TE solutions have been investigated for a wider range of urethral strictures. Over the past, various combinations of cells and scaffolds have been the focus of some successful studies [25]. It is generally accepted that cell-loaded grafts significantly reduce the incidence of strictures, fistulas, and infections [69]. Also, cellularity promotes the growth of blood vessels and urethral barriers, thereby reducing local inflammation and fibrosis associated with urinary leakage [6]. Therefore, the selection of the appropriate cell type and associated scaffold is crucial in tissue engineering for urethral repair.

The urethra is anatomically composed of the renal pelvis, ureter, bladder, and urethra. It is involved in the transport of urine from the kidneys, physical excretion, and bodily drainage [70]. Histologically it consists of three different layers including the epithelium, the connective tissue that forms the submucosa and the external smooth muscle [71]. The muscular layer consists of smooth muscle cells and is primarily responsible for producing the coordinated waves of contraction that are necessary for the transport and excretion of urine. The submucosa is formed by an extracellular matrix containing blood vessels, lymph, nerves, and various cells. Of these, fibroblasts play an important role in the formation of the submucosa. Therefore, cell-based studies of urethral remodeling have focused on the three important target cells mentioned above. They are divided into two categories according to their different cellular origins: progenitor cells and stem cells.

Table II. Cell sources used for urethral tissue engineering. Detailed description of properties of each cell type can be found in Appendix I.

Progenitor Cells	Stem Cells
Epithelial cells [72–75]	Embryonic stem cells [76,77]
Smooth muscle cells [78,79]	Induced pluripotent stem cells [80,81]
Fibroblasts [82,83]	Bone marrow stem cells [84,85]
Epidermal cells [86,87]	Adipose-derived stem cells[57,88]
Mesothelial cells [89]	Urine-derived stem cells [90]
	Hair follicle stem cells [91]
	Amniotic fluid stem cells [92,93]

The selection and application of cell types requires consideration of a range of parameters: the ability of the cells to proliferate *in vitro*, their ability to be immunomodulated and the damage they cause to the patient during collection. While a variety of progenitor cell types have been explored for urethral tissue engineering, urothelial and smooth muscle cells remain the main cell types in the field of urethral regeneration due to their key role in maintaining structure and function. Despite the wide range of sources of urothelial cells and the many successful experiences with urothelium obtained by bladder biopsy, the use of urothelial cells is further limited by the trauma of surgical interventions to the bladder and urethra. Recent studies have shown that it is possible to extract urothelial cells non-invasively from bladder irrigation fluid and urine [73]. As the most important cell type in the muscle layer, smooth muscle cells appear to have an irreplaceable role in urinary tract regeneration, as they play a unique role in regulating caliber elasticity, preventing wall adhesions and lumen collapse [78].

Stem cells have the capacity for self-renewal and differentiation, providing an additional source of cells for urinary tract regeneration. In contrast to the ethical limitations of embryonic stem cells, adipose-derived stem cells have the advantage of multiple cell sources and are candidates for this field. Researchers have proposed several approaches to stably induce the differentiation of adipose-derived stem cells into epithelial [94,95] and smooth muscle phenotypes [96,97]. In addition, adipose-derived stem cells secrete a variety of bioactive molecules that contribute to angiogenesis and wound healing, which are particularly important for regenerating the urinary tract and inhibiting fibrosis [98]. Stem cells derived from urine have the advantage of being non-invasive and low-cost and have received increasing interest from researchers in recent years [90]. It is also better adapted to the urine environment and ensures cell viability due to its inherent advantage of contact with urine. However, the related extraction and preservation techniques still need further research. A more thorough analysis of cell sources for urethral tissue engineering is provided in the Appendix I of the thesis.

2.4.3. General biofabrication techniques for urethral TE

In addition to biomaterials and cells, various biomanufacturing strategies have been developed which play an important role in the final graft performance. Traditional biomanufacturing strategies including solvent casting, freeze drying, and gas foaming have a number of limitations in their application. Firstly, there is limited control over scaffold structure and uniform cell distribution cannot be achieved [99]. In addition, angiogenesis and nutrient delivery is hindered, ultimately leading to low graft success rates [100]. Finally, the complexity of the experimental steps and the length of time required seriously affect the efficiency of the application of tissue-engineered urethra. In order to better simulate the physical natural environment and improve the success rate of transplantation, a number of new techniques have been developed and applied in the field of urethral tissue engineering in recent years.

Electrospinning is an electrostatic fiber fabrication technique produced by applying an enhanced electric field to a polymer solution or melt. Compared to conventional techniques, the experimental process is relatively simple and the resulting nanofibrous scaffolds are produced near the extracellular matrix composition, thus showing more interest and interest in urethral tissue engineering [101–103]. In-situ tissue engineering technology is a combination of biodegradable biomaterials to enhance the regenerative potential of the body through rational scaffold design (including structural optimization and functionalization), ultimately leading to the reproduction of natural tissue regeneration. The application of this technology in the field of urethral regeneration has been successful, but the long-term success rate still needs further research [51,104]. 3D printing technology has attracted a great deal of attention in recent years as a powerful tool in the field of regeneration. It allows the design and manufacture of a variety of cellular and matrix structures with site-specific properties that mimic the complex structure of natural tissues, depending on the specific needs of the patient, which are not possible with general tissue engineering techniques [10]. A variety of technologies have been successfully developed in 3D bioprinting. At the same time, it has become an important part of the field of urethral tissue engineering due to its obvious technical advantages. Some more detailed insights about current strategies for preconditioning cells for urethral tissue engineering are provided in the Appendix I of the thesis.

2.5. 3D bioprinting

As an advanced technology in the field of TE, 3D bioprinting has the potential to enable the creation of personalized, patient-specific designs, producing high-precision, efficient, and cost-effective complex structures on demand by depositing cells and biomaterials on a layer-by-layer basis [105].

2.5.1. 3D bioprinting process

In brief, the envisioned process or 3D bioprinting based therapy follows three basic steps: In the first stage, a personalized treatment plan is developed based on patient information from magnetic resonance imaging (MRI) or micro-computed tomography (μ-CT scans).

An accurate 3D model is designed using computer graphics software (CAD) and transferred to a bioprinter for printing. At this stage, biomaterials and cell types need to be selected and developed as needed to match the biological characteristics and printing requirements. In the second stage, the tissue construct is printed using the mixture of hydrogel and cells also known as the bioink. In this process, a range of printing parameters including temperature, speed, and pressure need to be optimized to obtain a 3D construct with a well-defined geometry. The third stage focuses on characterizing the cell viability, proliferation capacity, and differentiation and maturation capabilities of the cell-filled 3D constructs [106,107].

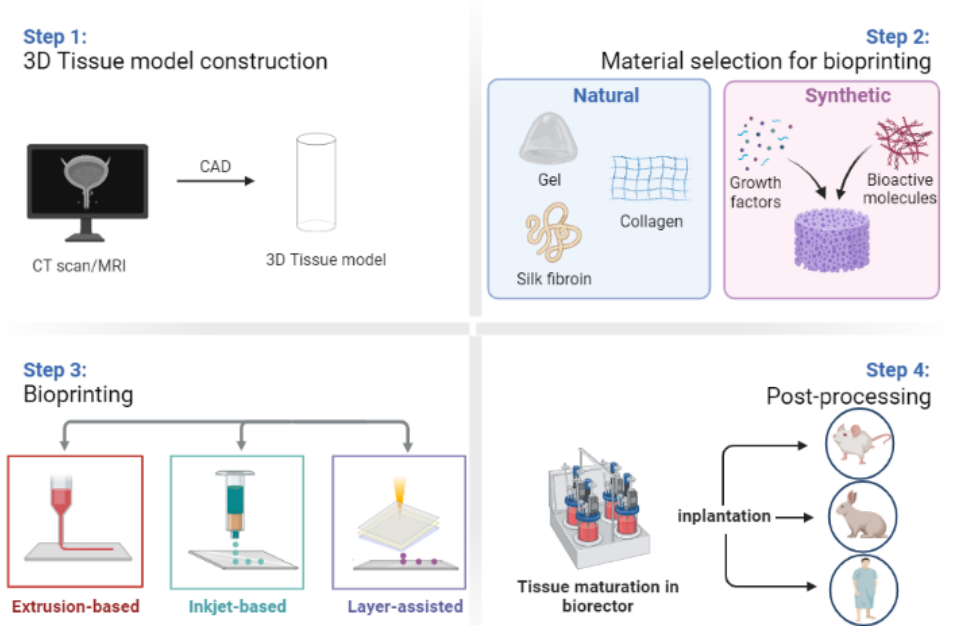

Figure 4. The typical 3D bioprinting process. Through computer-aided design, medical images are converted into STL files as part of preprocessing. Additionally, the choice and preparation of the bioinks need to be done. Using a bioreactor, tissue maturation and remodeling may be accomplished following the bioprinting procedure. The tissue can be transplanted into the patient once it has finished developing to restore tissue function. Figure created with BioRender.com

2.5.2. Types of bioprinting

Various printing technologies have been investigated and there are now three main technologies that have made great progress in the field of TE (Figure 4). Inkjet bioprinting, the first bioprinting technology to be applied to TE, achieves printing through a non-contact process, specifically the deposition of small precise drops of 'bioink' onto a hydrogel matrix or culture dish at predetermined locations. The advantages of inkjet bioprinting are low cost, high resolution, and high efficiency. However, this method is difficult to apply to highly viscous bioinks as it is limited by the fact that only very small forces can be used to eject the droplets [108].

Laser-assisted bioprinting is based on the use of a laser as an energy source to deposit biological material onto a glass sheet. The technique usually consists of three parts: (i) a pulsed laser source device, (ii) a strip coated with liquid biomaterial and deposited on a metal film, and (iii) a receiving substrate [109]. This technique is effective in avoiding the effects of nozzle clogging and shear stress on the nozzle wall on cell viability. However, its high cost and low efficiency limit its widespread use.

Extrusion-based bioprinting is currently the most used bioprinting strategy because of its versatility in printing 3D structures [110]. It is mainly controlled by a computer-controlled fluid distribution system, where the bioink is extruded in a continuous manner through micro-nozzle holes or micro-needles in filaments that reach a designated substrate through a coordinated movement of air pressure. After layer-by-layer deposition of the biomaterial, the final result is a complete three-dimensional pattern and structure. Although factors including the size, type, pressure, and speed of the print head have been greatly improved to accommodate different bioink properties [111]. However, the strategy still has some limitations. The resolution of the constructs is much lower than inkjet or laser-assisted bioprinting; furthermore, the printing process always requires high print speeds, but complex 3D structures often take a long time to complete the printing process. Cells must wait a long time before they can be cross-linked, and the prolonged media-free state can seriously impair cell viability [112]. Overall, extrusion-based bioprinting offers the possibility to print 3D constructs with satisfactory shape fidelity, however, bioinks and printing methods adapted to different cells and different printing conditions need further development.

2.5.3. The concept of bioink

Bioinks are materials used to produce engineered artificial living tissues using 3D printing technology. These inks consist mainly of living cells and biomaterials that mimic the extracellular matrix environment, while possessing rheological, mechanical, biofunctional properties to support the stability of the structure of the printed construct and to promote cell adhesion, proliferation, and differentiation [113]. Unlike conventional 3D printing materials, the printing conditions for bioinks are more stringent to maintain cell viability: i) printing temperatures should not exceed physiological temperatures; ii) mild cross-linking conditions; and iii) a sterile environment should be maintained throughout the printing process.

2.5.4. Influence of bioink properties and printing parameters on print fidelity and cell viability/ functionality

Two main aspects of hydrogels - physical quality and biological properties - have been considered in the development of bioinks loaded with 3D structures for printing cells. Physically, the bioink should have gelling properties when extruded from the tip of the nozzle and have a solidified filament morphology, and it must be mechanically strong enough to support the deposition of additional layers [114]. Biologically, the bioink should provide a suitable microenvironment to support various cellular activities such as migration, proliferation, differentiation, and the generation of specific tissues [115]. The printability of the bioink, the ability to form 3D structures with good fidelity and integrity,

and the viability of the cells, i.e., their ability to survive after printing, represent criteria for physical and biological properties respectively. An ideal bioink with optimal rheological properties should also maintain cell viability after printing and cross-linking.

Increasing the concentration and enhancing the cross-linking effect of bioinks can both improve their printability and the stability of the 3D structure. However, this strategy also significantly affects the stiffness of the bioink, which plays a crucial role in cell behavior. For example, mesenchymal stem cells (MSCs) differentiate into bone cells when grown on stiffer substrates (~40 kPa) and into neural cells on softer substrates (~1 kPa) [116] . One of the key factors in the success of bioprinting is related to the rheological properties of bioinks. High concentrations of bioinks often lead to cellular deformation and damage, as higher viscosity bioinks tend to require higher pressure compression, a process that can severely impair cell viability. In addition, after cross-linking, the porosity of the cellular matrix formed by the high concentration of bioink is reduced, thus limiting cell migration and nutrient transport.

On the other hand, a low viscosity bioink can be printed at very low pressures and also helps to maintain cell viability. However, it often has extremely poor shape fidelity and cannot achieve the goal of printing multi-layer structures. Researchers have therefore undertaken a series of experiments based on low concentration bioinks to improve the shape fidelity of 3D constructs while ensuring cell bioactivity. In this direction, the development of combinations of bioinks is currently a promising solution. It can synergistically support printing by exploiting the joint advantages of two or more hydrogels in terms of cellular behavior and printing performance.

The success of bio-printing also depends on other factors such as the performance, size and type of print nozzle. Due to the viscosity of the bioink itself and temperature variations, bioink can easily clog the nozzle during printing. It is therefore also very important to choose the right nozzle size [100]. Crosslinking methods and times are also factors to consider. Cumbersome crosslinking methods and excessively long crosslinking times will seriously affect the viability of the cells [117]. The density of cells mixed with the bioink is also a current research topic, as there is evidence that high density cell seeding facilitates connections between cells at a later stage, thus further promoting cell maturation and differentiation [118]. However, low density cell seeding is more conducive to observing and comparing experimental results, such as initial cell viability [119].

2.5.5. Considerations about bioinks for bioprinting smooth muscle cells

Considering the ability of 3D bioprinting to fabricate cell-laden 3D constructs in a rapid, and straightforward manner, a wide variety of hydrogel-based biomaterials have been investigated for use as bioinks. Here the focus will be placed on three potential candidates for 3D bioprinting of smooth muscle cells for urinary tract regeneration: alginate, collagen, and gelatin methacrylate.

Alginate is a natural biopolymer derived from brown algae and its unique double monomer repeating unit structure facilitates gel formation requiring simple ionic crosslinking to

complete the gelation process[120]. The viscosity of the alginate hydrogel can be adjusted by varying the concentration and cross-linking time to achieve a stable 3D printed construct structure. In addition, alginate offers a range of advantages such as water retention ability, biocompatibility, and low cost, making it the material of choice for many 3D bioprinting applications [121,122]. Numerous alginates have been developed for use in tissue engineering, including urethral regeneration [123,124]. However, despite their printing advantages, alginate hydrogels can be prepared in a very limited concentration range (2-4%) because of the effect of porosity on cell viability [125] . Even though lower alginate concentrations ensure higher cell survival, cells tend to exhibit poor cell adhesion in the gel as the polysaccharide does not contain cell-specific adhesion ligands, limiting further cell maturation and differentiation. In addition, the slow degradation kinetics of hydrogels limit their further application in the field of regeneration [121,126].

Collagen is the most abundant protein in the ECM and can be obtained from natural biological materials [127]. As a protein with a specialized fibrous structure, it plays an important role in supporting the mechanical properties of the ECM. There are several examples of the use of collagen scaffolds. On the other hand, collagen has been also used as a bioink for 3D bioprinting due to its good biocompatibility and biodegradability and low immunogenicity [128]. However, collagen gels need to be cross-linked at 37°C before achieving a stiff structure, and too long a cross-linking time can affect the shape of the constructs [129]. More importantly, although collagen can exhibit higher mechanical strength and viscoelasticity after cross-linking, its mechanical properties are not easily customizable, to adapt the bioink the specific cell or tissue type. For this reason, current research is focused on how to improve the mechanical strength of collagen scaffolds by adjusting the cross-linking method or by selecting other materials to be combined with collagen. On top of this, several attempts have been made to add biochemical factors to the scaffold to improve cell viability [130].

Gelatin has gained some attention due to its collagen origin, and cells embedded in gelatin scaffolds have enhanced biological properties compared to synthetic materials, providing good biodegradability, biocompatibility and thus effective tissue integration between the scaffold and the cells [131]. Gelatin is obtained from denatured collagen, which makes the material biocompatible and biodegradable for use in *in vitro* cell growth [132]. Gelatin itself can form a gel-like structure, but its relatively low melting temperature greatly limits its use in tissue engineering applications [133]. One strategy is to use photopolymerization, where cross-linking is accomplished by the addition of methacrylate [134]. Lysine functional groups on gelatin structures formed by methacrylation of methacrylated gelatin (GelMA) retains good bioactivity and can be cross-linked to form stable structures by simple UV exposure. This strategy can greatly improve the mechanical properties of gelatin and the effect can be adjusted by the intensity of the photopolymerization and the concentration of the bioink. Gelatin-methacrylate (GelMA) can take full advantage of the good biocompatibility of gelatin, combined with controlled photopolymerization, resulting in precisely constructed three-dimensional structures. As a result, GelMA is currently being developed and used extensively in the field of tissue engineering. However, the optimal conditions to allow cell maturation and extracellular base taking advantage of the GelMA-based base are still unknown, and since the requirements for cellular activity and the viscosity required for bioprinting are often in conflict with each other, it remains a

challenge to optimize the GelMA concentration to achieve a balance between cell viability and printability.

2.5.6. The effect of mechanical signaling on the regulation of SMC phenotype and differentiation capacity

In addition to soluble biochemical factor signaling, cells *in vivo* have also been shown to be influenced by the mechanical properties of the ECM. Therefore, studies have focused on how cells respond to the mechanical properties of polymeric scaffolds. By varying the mechanical properties of the polymeric scaffolds, studies have shown the effect of matrix stiffness on cell spreading and motility[135]. These results have shown that cells on less stiff matrices spread less and are more motile. On the other hand, cells on substrates with higher stiffness show stronger dynamic focal adhesion. By altering collagen fibers at the nanoscale, McDaniel and coworkers showed that SMCs exhibit a synthetic phenotype and a rapid proliferation rate[136]. Another study by Yi et al. confirmed similar results. They found that when the stiffness of scaffolds was increased, that resulted in downregulation of contractile indicators such as -smooth muscle actin (α- SMA), myosin smooth muscle heavy chain, calmodulin and desmin, while gene expression of pathologically associated osteopontin (OPN) was upregulated[137] Therefore, it is important to consider not only the printability when preparing SMC-based bioinks, but also the possibility that stiffness may alter the phenotype of SMCs.

The urethra is functionally and structurally a dynamic organ that tends to perform a series of necessary mechanical stretches on the SMCs during the urinary cycle. Previous studies have shown that mechanical stimulation plays a key role in the regulation of smooth muscle cell phenotype [138], structure, and function [139], and even the effects on cell survival [140]. To meet the physiological functional and structural requirements of the graft, a range of mechanical stimulation techniques have been developed to mimic the physiological mechanical environment *in vivo*.

As a common method to mimic the cyclic circumferential strain experienced by SMCs *in vivo*, cyclic tensile strain (CTS) specifically mimics the cyclic mechanical strain experienced by SMCs *in vivo* by applying mechanical stimulation to cells through alternating phases of stretch/relaxation and relying on the adjustment of stretch parameters, amplitude, and duration. Back in 2000, Nguyen et al. used the FX-4000T strainer to cyclically strain rabbit bladder smooth muscle cells for 4 h at 0.1 Hz and 25% maximum strain setting and found that mechanical stimulation promoted DNA synthesis and gene expression in normal bladder smooth muscle cells[141]. More recently, Chae et al. introduced mechanical stimulation to 3D printed engineered bladder smooth muscle tissue and found that mechanical stimulation played a role in promoting myogenic differentiation potential under 3D conditions [142].

Understanding the mechanisms of action of mechanical stimuli in organisms that affect cell proliferation and differentiation is particularly important for the situations that grafts need to face. It has been proposed that the cellular response to mechanical forces occurs through a mechanotransduction process that transmits mechanical stimuli to the cell surface to the nucleus via various intracellular signaling pathways, and that this

biochemical signaling leads to the activation of signaling pathways that further affect cell proliferation, gene expression or cell death[143]. A previous study has shown that mechanical cycling activates the Rac1 pathway and its downstream mitogen-activated protein kinases (MAPKs). MAPKs are a family of serine/threonine kinases that include extracellular signal-regulated kinases (ERKs), c-Jun NH2-terminal protein kinases (JNKs) or stress-activated protein kinases (SAPKs) and p38 MAPK. Cyclic stretch stimulates DNA synthesis and gene expression in normal bladder SMCs through multiple independent receptor systems and at least one MAPK pathway (p38 SAPK2) [141]. Similarly, Rosalyn et al. had imposed cyclic stretch stimulation by using p38 stress-activated protein kinase 2 (p38SAPK2) as a mediator of gene expression changes and DNA synthesis in rodent bladder smooth muscle cells (SMC). The results show that this effect is mediated by signaling through the p38 pathway and can be abrogated by p38 inhibitors [144].

2.4. Current status of urethral TE

Due to the important role of the muscle layer in urethral regeneration, conditions that promote the maturation and differentiation of smooth muscle cells are of increasing interest. In addition to the mechanical properties of the hydrogel itself, mechanical stimulation has been shown to play an important role in the maturation and differentiation of muscle cells. Although previous studies have shown that mechanical stimulation promotes DNA synthesis in bladder smooth muscle, studies have mainly focused on two-dimensional culture environments, whereas cells grow and mature in the three-dimensional environment of the human body. While there is evidence that indicates that mechanical stimulation promotes myogenic differentiation under 3D conditions [142], the mechanisms underlying this regulatory effect are not yet clear. Furthermore, the application of cyclic stretch tends to be uniaxial, whereas the mechanical stimuli received by cells in the urinary tract *in vivo* is typically from all directions. In addition, studies have typically focused SMCs of arterial or pulmonary origin, and the cells are mainly in a 2D culture environment[145].

CHAPTER 3. OVERVIEW OF PHD PROJECT

The hypotheses of the PhD project are:

1. A suitable hydrogel and cells combination can be bioprinted to create 3D structures *in vitro* that mimic the structure of the urethra.

2. Mechanical signals play a key role in the differentiation of the cells in the urethral smooth muscle layer.

In order to test these hypotheses, the project has the following objectives:

Objective 1: To develop an *in vitro* model of the urethral smooth muscle layer using a novel 3D bioprinting approach

Objective 2: Using the model developed in Objective 1, to investigate the effects of cyclic mechanical strain on smooth muscle cell differentiation.

To address these objectives and test the hypotheses, two studies were designed and conducted as described below and outlined in Figure 5:

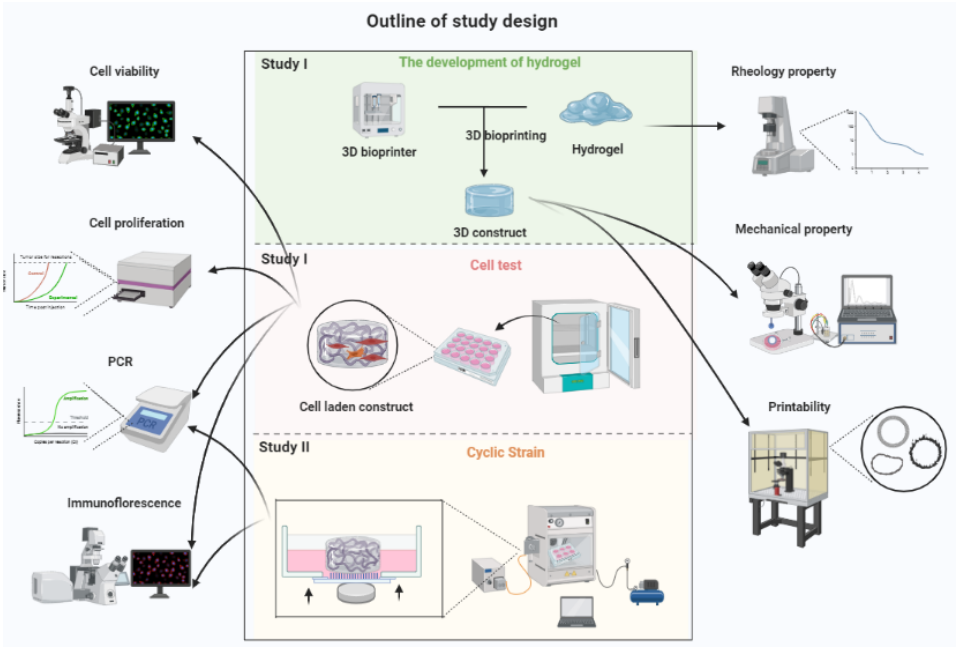

Figure 5. Outline of study design. In Study I, the physical properties of the hydrogels, printability, effects on cell viability, proliferation and differentiation were characterized before and after printing. In Study II, the effect of mechanical stimulation on the differentiation capacity of the cells is characterized under 3D culture conditions in hydrogels. Figure created with BioRender.com

CHAPTER 4. Materials and methods

In this section, the rationale for the choice of materials and methods will explained or discussed. Table III summarizes the key experimental methods applied in each experimental study. Further specific description of the methodological steps and materials are presented in the papers corresponding to each study (Appendices II and III).

Table III. An overview of methodologies applied in the individual studies.

Study	**Study I**	**Study II**
Preparation of hydrogel	*	*
Characterization of bioinks (Rheology, mechanical properties, printability, and stability)	*	
Cell culture	*	*
3D bioprinting	*	*
Cell viability (live/dead)	*	
Cell proliferation	*	
Cell differentiation (PCR/immunofluorescent staining)	*	*
Surface modification of PDMS		*
Cyclic strain		*

4.1. Selection of cells

Different cell types have been used for tissue engineering of the urethra. The current research in this field was reviewed by comparing cell sources, proliferation capacity, and maturation potential (Appendix I). Primary smooth muscle cells (SMCs) are of key importance since they contribute to mechanical integrity of the urethra. Adipose-derived stem cells (ASCs) have shown promise as cell type for urethral regeneration because they are readily accessible, have potential to differentiate into urothelial and smooth muscle cells, and can secrete a variety of bioactive molecules. Therefore, in the beginning of this PhD project we focused in comparing these two cell types.

In initial experiments, the ability of SMCs from human bladder and ASCs to differentiate into the contractile smooth myogenic phenotype in tissue culture plates was compared. Specifically, human ASCs were plated and grown to confluence in growth medium (GM, alpha-MEM supplemented with 10% FBS, 100 IU/mL penicillin and 0.1 mg/mL streptomycin). The GM was then replaced with smooth muscle differentiation medium (DM1, alpha-MEM supplemented with 1% FBS, 5 ng/mL TGF-β1, 2.5 ng/mL BMP4, 100 IU/mL penicillin and 0.1 mg/mL streptomycin) and differentiated for 2 weeks. Finally, the smooth muscle differentiation medium was replaced with smooth muscle specific differentiation medium (DM2, Ham's F12 supplemented with 1% FBS, 30μg/ml heparin, 100 IU/mL penicillin and 0.1 mg/mL streptomycin) and the differentiation culture continued for 10 days. In parallel, bladder smooth muscle cells were first cultured in smooth muscle growth medium for 10 days (Ham's 12 supplemented with 5% FBS, 5μg/ml Insulin, 0.5ng/ml EGF, 12ng/ml FGF-b, 100 IU/mL penicillin and 0.1 mg/mL

streptomycin) and then replaced with smooth muscle specific differentiation medium (DM2, Ham's F12 supplemented with 1% FBS, 30μg/ml heparin, 100 IU/mL penicillin, and 0.1 mg/mL streptomycin) for 10 days.

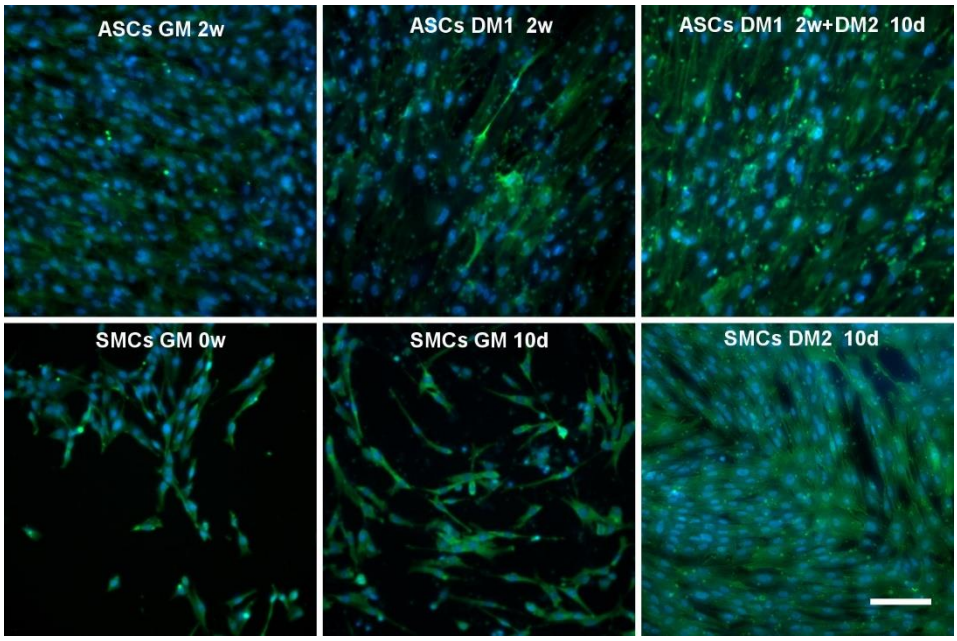

Figure 6. Comparative characterization of the differentiation capacity of ASCs and SMCs. (Immunofluorescence images. Green: α-SMA; Blue: Nuclei. Scale bar: 100μm)

At different time points cells were fixed and the differentiation level was evaluated by means of immunofluorescence staining (Figure 6). By comparing the expression levels α-SMA, we found that bladder SMCs displayed a more intense and uniform differentiation pattern than ASCs under the same conditions. Furthermore, the differentiation process of SMCs was simpler and less time-consuming. Considering that the subsequent experiments were in the *in vitro* model establishment stage, we chose bladder SMCs as the cell type for the subsequent experiments.

4.2. Development of bioinks for 3D bioprinting

4.2.1 From pure GelMA to blend hydrogels (GelMA/Alginate)

The development of cell-laden hydrogels is the focus of tissue engineering. In particular, gelatin methacrylate (GelMA) is currently a popular candidate due to its ability to mimic the natural muscle tissue environment and tunable properties [146].

Previous studies have shown that low concentrations (i.e., $\leqslant$5 w/v %) of GelMA can maintain high cell stability and viability [147]. However, its application is mainly limited by its low viscosity, which does not allow the creation of 3D constructions with high precision geometry. Even after curing, it still does not have sufficient mechanical strength

to maintain the pre-defined geometry [148]. In contrast, GelMA at high concentrations (i.e., >15 w/v %) presents excellent printability due to its high viscosity, but the high mechanical strength required after curing limits the reaction and behavior of the cells in the bioink [149]. Therefore, one of the biggest challenges for GelMA applications in tissue engineering is to balance printability with biofunctionality.

Based on the above findings and to explore the GelMA concentration suitable for 3D bioprinting, GelMA lyophilized from Cellink (Cellink AB, Gothenburg, Sweden) was used in the initial phase of the PhD and GelMA hydrogels were prepared at 5%, 10% and 15%. After mixing with SMCs, a ring-shaped model of the urethral smooth muscle was fabricated using a 3D bioprinter. The geometry of the model and its cellular response and behavior were evaluated. The results showed that 5% GelMA required low pressure to extrude through the printer nozzle due to its low viscosity. Despite attempts to increase PI concentration and UV curing time within a certain range, it was still difficult to build and maintain a highly accurate scaffold shape. On the other hand, the 15% GelMA exhibited low cell viability in the first three days after printing. This was as expected to understand since 15% GelMA usually requires higher pressure to be extruded, and high pressure may affect cell viability. In contrast, 10% GelMA appeared to strike some balance between printability and biofunctionality, but was still not viscous enough for bioprinting. In addition, GelMA hydrogels were extremely sensitive to temperature changes in the printing environment, and the shape of the hydrogel could change slightly during printing, which could lead to nozzle clogging. A possible solution to the above limitations was to add a different material to improve the printability of the bioink while maintaining high cell viability with a lower concentration of GelMA.

Alginate is widely used in tissue engineering due to its biocompatibility and low cost. Alginate has been shown to interpenetrate GelMA to improve its mechanical properties. While alginate does not have intrinsic cell adhesion motifs (i.e., RGD peptide sequence), GelMA can provide an RGD pattern for cell attachment to functionalized alginate and thus become a matrix to which cells can adhere [150]. Thus, the combination of GelMA and alginate provides an opportunity to improve the bioink formulation for tissue engineering. While it is possible to find commercial formulations of GelMA/alginate, their compositions are undisclosed.

Although alginate can increase the strength of GelMA, excess alginate also reduces the biofunctionality of the blend bioink. Therefore, it is important to choose a suitable concentration range for alginate. Zhu et al. investigated the printability of hybrid hydrogels with different alginate concentrations based on a 7% GelMA hydrogel. Their team concluded that the alginate concentration should generally be controlled in the range of 1-5% [125]. Further combined with the range of shear rates obtained from Cellink's viscosity tests for different concentrations of alginate (1%, 3% and 5%), we chose alginate concentrations of 1.5% and 3% respectively. Considering the advantage of low concentrations of GelMA in preserving cell viability, the final experimental groups were set at GelMA/alginate concentrations of G1 (5/1.5), G2 (5/3), G3 (7.5/1.5) and G4 (7.5/3). G5 consisted of pure GelMA (10%) and served as a control group.

4.2.2. Preparation of the hydrogel

The preparation of hydrogels was mainly divided into three stages. In the first stage, the alginate (Sigma-Aldrich) was first dissolved in PBS at room temperature. As this solution had to be mixed with the GelMA hydrogel in a 1:1 ratio, the concentration of dissolved alginate powder at this point was twice the final required concentration. During the sterilization phase, it is not only important to ensure optimal sterility of the hydrogel, but also preserve as much as possible the physical and chemical properties of the hydrogel for bioprinting. On this basis, and by comparing the main methods of autoclaving, ethanol washing and UV irradiation, UV irradiation was the alginate sterilization method that met our experimental requirements [151]. Briefly, after complete dissolution of the alginate, the hydrogels were placed in a Stratalinker 1800 UV crosslinker (Stratagene, California, USA) and irradiated for 20 mins at with a UV wavelength of 250 nm.

In the second stage, the appropriate concentration of reconstituted photoinitiator was first prepared according to the protocol recommended by Cellink. Although the LAP concentration commonly used in bioprinting (<0.5% w/w) has not been shown to be cytotoxic, high concentrations of LAP can also cause varying degrees of damage to cell membranes [152]. In conjunction with the recommended concentrations of Cellink products, we chose a concentration of 0.25% for the LAP solution. Using a sterile 0.22 µm syringe filter, the PI solution was filtered into a sterile15 ml Falcon tube and used to dissolve the GelMA lyophilizate.

In the third stage, the two hydrogels were mixed thoroughly mixed in a 1:1 ratio and the mixed hydrogels were stored away from light. All hydrogels are stored at 37°C until further use. Different storage conditions may affect the properties of the hydrogels. We tried storing them at 4°C for 1 week and then warming them before the experiment. The rheological tests showed a significant change in the properties of the above stored hydrogels compared to the freshly formulated hydrogels, while the properties of the hydrogels stored in the incubator at 37°C for a short time did not change significantly.

4.2.3. Characterization of hydrogels

Once the bioink was developed, the printing conditions had to be optimized to maximize the resolution and reproducibility of the process. Among the parameters that influence the printing process, the rheology is an important aspect. In conjunction with the important role that the mechanical properties of bioinks play in influencing cell proliferation and maturation, the rheological and mechanical properties of hybrid bioinks were tested in Study I.

4.2.3.1. Rheological properties

The printing temperature (28°C) was first set under the AR-G2 rheometer (TA Instruments, New Castle, DE) operating system and mechanical spectroscopy was performed over a frequency range of 0-100 rad s^{-1} to assess the stability of each group of hydrogels at the original printing concentration. A temperature scan was then performed to cool the GelMA solution from 37°C to 2°C at a cooling rate of 5°C/min to assess the effect of different hydrogel combinations on the gelation process. As the gelation process is time-dependent, further time scans were performed at 28°C (printing temperature) and

10°C (platform cooling temperature) to obtain the gel state of all gel combinations during the printing and cooling phases respectively.

4.2.3.2. Mechanical properties

To further quantify the mechanical properties of different hydrogel combinations after curing, we applied a commercial nanoindenter (Chiaro, Optics11). The device can assess sample deformation by detecting and quantifying the degree of cantilever bending during indentation. The instrument is equipped with a cantilever beam connected to the system by an optical fiber that scans the sample with the probe tip. The cantilever ends when the probe contacts the sample, and the optical fiber in the probe can record and detect this change in displacement. Through a series of non-destructive analyses, the corresponding results are displayed graphically and mathematically in the Optics 11 software.

In preparing the test samples, two methods were used. First, we used a dropping method to directly deposit the hydrogel directly onto the surface of a Petri dish. This method was easy to handle, the shape of the sample was easy to control, and the surface was uniforms. However, the spherical shape of the droplet was an issue since indentations should be made on a horizontal surface. The probe tip is very sensitive to the uppermost area of the droplet, so the area in which measurements can be made is extremely limited. As a second approach, we used Sigmacote-modified coverslips to help solidify the hydrogel. This method could ensure the flatness of the surface of the hydrogel. However, when the coverslip was removed, tiny defects appeared on the surface of the hydrogel. At the same time, when the coverslip is removed, the cured hydrogel could easily detach from the surface of the Petri dish. Since the measurements are typically performed in solution, it is important to ensure that the sample adheres to the surface of the test platform. To this end, a 20-mm microwell was created in an ordinary 35-mm glass-bottomed Petri dish and pipetted 60 µl of the hydrogel sample into the microwell, which, together with the coating of a cover glass, forms a thin, flat structure. The microwell effectively prevented the sample from detaching when the coverslip used to flatten the hydrogel was removed.

Before calibration began, the integrity of the probe and the absence of air bubbles on the top of the probe were checked to ensure that wave propagation between the cantilever and the light was maintained. A new calibration procedure was performed each time the liquid environment was changed. The calibration procedure first ensured that the probe was fully immersed in the liquid to avoid interference from surface tension. After a signal of normal strength was found, the instrument was activated to search for the surface, and when the surface was found, the calibration factor was determined.

After setting the displacement control, the search for the surface was performed again before the test, and the probe stopped a few micrometers above the surface. Then the actual measurements were performed. The displacement control mode was run to ensure that the initial Hertzian fit of the load indentation curve began at a load of zero. The matrix indentation mode was activated and each specimen was indent 25 times in a 5 x 5 matrix scan with each indentation point 30 µm apart to measure the elastic modulus. The effective elastic modulus was calculated and the Hertzian model was used to determine the distribution of the elastic modulus over the surface.

4.3. Cell source

The human bladder SMCs used in the two experimental studies of this thesis were obtained from two different suppliers. In the first study, the primary SMCs from were able to mature and differentiate in the hydrogel. However, after few passages, the cells appeared to decline their proliferation rate significantly and, more critically they lose their ability to differentiate. The human smooth bladder cells used in the second study were from the ATCC (LGC standards). Interestingly, under the same hydrogel combination conditions, the differentiation of these cells appeared to be more prominent. The specific culture procedure was described in a separate manuscript and is not repeated here.

4.4. 3D bioprinting procedure

In Study I, the bioinks consisted of different concentrations of GelMA and alginate, 0.25% (w/v) photoinitiator (LAP) and human bladder SMCs. The cross-linking solutions contained 0.1 M CaCl2 and were prepared in Milli-Q water. For better observation of cell spreading, a relatively low cell density (2 x 10^6 cells/ml) was used in the experiments. Circular muscle layers are widely observed *in vivo* (e.g., the external urethral sphincter) and are essential for the maintenance of physiological processes. The structural organization of these muscle cells plays an important role in regulating cell patterns (spatial distribution of cells) and cellular arrangement to maintain muscle function. To simulate the circular external urethral sphincter *in vitro* [153], a circular 3D structure with a diameter of 3 mm was designed and built at this stage, considering the actual diameter range of the urethra. Due to the sensitivity of GelMA to printing temperature, a temperature-controlled print head was chosen for the experiments. When it came to the choice of nozzle and needle, we favored the latter. Although plastic nozzles are easier to extrude hydrogels, due to the properties of GelMA, the nozzles can easily get clogged during the actual printing process. Considering the dual evaluation criteria of biofunctionality and printability, a needle with a diameter of 0.20mm was finally chosen for the experiment. Regarding the order of the two curing methods for hybrid hydrogels, previous study favored a strategy of ionic curing first, followed by UV irradiation [119]. However, after our comparison of the different sequences it was found that UV irradiation followed by ionic curing was clearly more beneficial for maintaining the geometry of the three-dimensional construct. In choosing the curing wavelength, a 405 nm light-curing module was used, as overexposure at 365 nm could damage the cells. In combination with the actual size of the 3D constructs, after comparing different curing times, the final decision was 15s for UV irradiation and 2mins for ionic crosslinking.

The hybrid hydrogel G4 developed in Study I was applied to Study II. At this stage we focused on testing the effects of mechanical stimulation on the maturation and differentiation of bladder smooth muscle cells and therefore applied a higher cell density. As printability was no longer a focus at this stage, a square 3D construct was developed and applied. The larger contact area between the square construct and the surface of the plate allows further strengthening of the adhesion between the 3D construct and the plate for mechanical stimulation. The relevant needle types and printing parameters have therefore been changed accordingly.

Table IV: Parameters of bioprinting process in the two studies.

Printing Parameters	Study I	Study II
Model	Ring-like structure (cylinder 3x0.6 mm)	Square-shaped structure (10x10x1 mm.)
Cell density	2 x 10^6 cells/ml	3 x 10^6 cells/ml
Print plate	Standard 6-well plate	Methacrylate-modified or amino-modified Bioflex plate
Print head	Temperature controlled	Temperature controlled
Nozzle inner diameter (mm)	0.20	0.33
Pressure (kPa)	18-25	16-20
Printing temperature (°C)	26-30	26-30
Cooling receiving platform temperature (°C)	10	10
Crosslinking method	UV (405nm) light 15s followed by 0.1 M CaCl2 ionic crosslinking for 2 mins.	UV (405nm) light 30s followed by 0.1 M CaCl2 ionic crosslinking for 3 mins.

4.5. Printability and stability

After the printing parameters have been defined, the study of print fidelity is an important part of assessing bioinks. Printability here is assessed primarily on the basis of the shape and size of the 3D constructs. Images of the constructs were taken immediately after printing and 14 days after 3D printing and crosslinking using the same type of needle, the same print environment, and close print factors under a microscope (Zeiss Lumar V12 Stereoscope) and AxioVision Rel (Carl Zeiss). Cellink XPLORE Cellink XPLORE is a test ink with good printability and adhesion developed by Cellink, was used as a control. The images were processed by Image J and the average cross-sectional area of each group of bioinks (6 samples per group) was divided by the average cross-sectional area of the control group to obtain the group of bioinks closest to the standard sample group.

4.6. Surface modification of PDMS

To verify the effect of mechanical stimulation on SMCs maturation and differentiation in 3D constructs *in vitro*, the 3D constructs were immobilized on the surface of the plate and mechanical stimulation was applied. However, the hydrophobicity of PDMS prevents it from achieving sufficient adhesion to hydrogels, limiting its applicability [154]. The current tissue dynamics studies applied to the Flexcell system mainly rely on the tissue train® culture plates, but these plates only allow uniaxial strain regimes, while cells in the urinary tract experience multiaxial strains.

Cha et al. A method to tune the adhesion of hydrogels to PDMS surfaces by covalently attaching alginate to PDMS surfaces is presented [155]. (Appendix II Figure 1) According to the protocol, we first modified PDMS with -NH_2 to achieve alginate adhesion. However, after repeated testing, the adhesion properties between the hydrogel and the plate surface

did not show a significant improvement. This may be due to our insufficient curing time, as too long curing time can severely impair cell viability. Another reason could be that we modified our original protocol and chose to cure the alginate layer before further curing with the constructs, mainly because the printer nozzle was unable to print effectively on the liquid hydrogel surface. This process may also have affected the curing effect as the alginate layer was not acting as a 'glue' to co-cure with the construct. In an alternative approach, we provide methacrylate after plasma treatment of the board surface and add a 20% solution of TMSPMA to help the hydrogel adhere to the board surface. The dilution solution we have chosen here is absolute ethanol. Compared to dilution with a toluene solution, anhydrous alcohol not only acts as a disinfectant but also provides a better environment for cell growth.

4.7. Cyclic strain

After 7 days of incubation with growth medium, all experimental groups were switched to differentiation medium. The static group was not used with circulating strains and the control group was discontinued. For the remaining three groups containing or not containing SB202190, the same cyclic stretching was applied to the cells using a computer-controlled vacuum stretching device (FX-5000T Tension Plus System, FlexCell International Corporation). Specifically, a standard circular piston with a diameter of 25 mm was selected for isometric strain. Based on previous study [156], the peak amplitude was set at 5%, the frequency at 0.1 Hz and the duration of the stretch pulse at 1s to maintain optimal proliferation and contractility of the bladder smooth muscle cells. Continuous stimulation and stretch cycles were performed at the same time for 1 hour each day for 6 days.

However, given factors such as the stretching device and the film thickness of the Flexcell plate, the actual peak amplitude acting on the cells may not match the theoretical value of the system setup. To test this hypothesis, experimental conditions were simulated. The plate was mounted in a Flexcell system and placed under a microscope (Zeiss Lumar V12 body lens) through this device. Different strain regimes (from 0 to 5% deformation) were gradually applied to the plate, and images of the 3D constructs on the membrane were captured at each stage with an AxioVision Rel (Carl Zeiss), with six photographs per set. The photographs were then analyzed using ImageJ software to obtain the cross-sectional area of the 3D constructs presented in six different states for each set of photographs. Using the static cross-sectional area as a reference, strain curves were obtained for different strain scenarios. By calculating the slope, the actual maximum strain applied to the construct in three dimensions for the strain scenario set to 5% was derived.

4.8. Cell viability assay

Staining of live and dead cells was performed immediately after printing, one day after printing, and seven days after bioprinting, respectively, to investigate how the printing process affects cell viability and how various mechanical properties affect cell spreading. Using Image J (NIH, USA), the number of live cells (green) and dead cells (red) was counted in each field of fluorescence images from six separate fields of the bioprinting construct. At least 100 cells were counted for each group, and the percentage of viable

cells was calculated using the following equation.

$$\%\text{Cell viability} = \text{live cells} \times 100/(\text{live cells} + \text{dead cells})$$

4.9. Cell proliferation within 3D constructs

A resazurin-based proliferation assay was used at different timepoints after bioprinting to assess the impact of various hydrogel groups on cell proliferation.

To the wells containing the cell constructs, 100 µl of Alamar Blue reagent (equivalent to 10% of the volume of medium per well) was added at each time point, and they were then incubated at 37 °C for 24 hours. Wells containing cell-free constructs served as negative controls. Then, 100 µl volumes were transferred (in duplicate) to 96-well microplates, where they were then analyzed for fluorescence using a multimode microplate reader (EnSpire, PerkinElmer). Fluorescence was observed at wavelengths of 560 nm for excitation and 610 nm for emission, respectively. After fluorescence measurement, the constructs were washed once with PBS, and then fresh GM was added.

Calculation of doubling time allowed comparison of cell proliferation rate based on measurement of fluorescence intensity. The reported mean fluorescence intensity was calculated by averaging the results obtained at each time point and subtracting the mean of the negative control. Using Microsoft Excel, the mean values for each group were then compared to an exponential trend in the form of a $Y = A \times e^{Bx}$ line fit, where Y represents the mean fluorescence intensity at time x, A the initial cell number, and B the frequency of unit time cell cycles. B is calculated, and t_d is calculated as $t_d = (\ln 2)/B$. The cell proliferation rate of each group can be calculated by comparing their td values.

4.10. Immunofluorescence staining

The SMC cell-containing constructs were cultured in growth medium for 7 days before transferring to differentiation medium (Ham's F12 medium supplemented with 1% fetal bovine serum, 30 g/ml heparin, and 1% P/S) for an additional 7 days. After fixation in formalin (10% neutral buffer) at 37°C for 15 minutes, the 3D cell- loaded constructs were blocked with 1% bovine serum albumin in PBS for 30 minutes at room temperature. Consistent with the antibodies previously used in the laboratory, diluted anti SMA antibody, anti-smoothelin, and anti-smooth muscle MHC from Abcam, Cambridge, UK, were used to characterize the different stages of smooth muscle cell development. Primary antibodies were incubated at 37 °C in a humid chamber. Secondary antibodies were then applied to the 3D constructs, which were incubated at room temperature for one hour. All groups displayed SMA positive cells, but none of the groups displayed positive smoothelin or MHC fluorescence. The fixation method and the duration of incubation of the primary antibody were systematically changed, while maintaining the other variables. Fixation was performed using 100% methanol as the new fixative for 5 minutes at room temperature. After the incubation time of the primary antibody was changed to 4 °C overnight, MHC showed positive fluorescence results in all groups to varying degrees. In contrast, the fluorescence of smoothelin remained negative in all groups. Therefore, this marker was not selected for further analysis. The area occupied by each protein (SMA and MHC) at

day 14 and the aspect ratio of the nuclei were further quantified using the previously obtained fluorescence images to evaluate the average cellular fluorescence intensity and cell morphology in each group of hydrogels.

4.11. qRT-PCR

To quantify the transcript levels of genes involved in SMCs differentiation, quantitative real-time PCR was performed in both Study I and Study II.

Different collection methods were used to obtain RNA in the two studies. In Study I, the constructs with cells were first removed from the culture plate and transferred to a microcentrifuge tube containing liquid nitrogen, which was ground to a powder. This process is difficult to manipulate and results may lead to significant RNA loss. Therefore, in Study 2 we chose Cell-Collect-A (Cellink) to solubilize the hydrogels to obtain higher quality RNA. In short, after removing the cell culture medium, Cell-Collect-A reagent was added to the desired wells. The entire well plate was placed on a cell shaker at room temperature for 2 hours to achieve complete lysis. The lysed ECM cell suspension was then filtered through a cell strainer, centrifuged for 5 minutes and the supernatant removed. For the RNA extraction phase, the Aurum Total RNA Mini Kit (Bio-Rad, Copenhagen, Denmark) was used in both studies.

RNA quality was measured using a spectrophotometer (NanoDrop; Thermo Fisher Scientific, Wilmington, DE, USA). Using the NanoDrop, the RNA measurement system was set up (260/280 nm) and 1 µl of RNA elution solution was used as a blank and 1 µl of sample was used to measure RNA concentration. Before cDNA synthesis began, we normalized the amount of RNA template to the sample with the lowest amount of RNA. Complementary DNA (cDNA) was synthesized using the iScript cDNA synthesis kit (Bio-Rad, Copenhagen, Denmark).

To assess gene expression at various stages of smooth muscle cell differentiation, five markers associated with smooth muscle contraction and two ECM-related markers were set as target genes. After testing a set of primers previously used in the laboratory [157], it was found that only *ACTA2* and *CALD1* were expressed normally in the bladder SMCs. Therefore, three additional target genes were redesigned. The procedure and criteria were as follows. In the NCBI web interface, a new "Primer-Blast" window was opened (see Table V for specific settings). In showing all primers, we followed the following reference criteria. a) Tm $\leqslant$ 63°C or CG < 70 %, and the Tm of both primers should be as similar as possible; b) no 4 similar nucleotides in a row; c) at most 3 C or G in the last 5 bases at both ends of the primer; d) A or T at the 3' end; e) selection of primer sets with low self-complementarity < 6.

Table V. Settings for designing primers.

Primer parameters	PCR product size: 120-150 Primer melting temperature (Tm): 60-63 °C
Exon/intron selection	Primers must be spaced from at least one intron on the corresponding genomic DNA
Primer specificity stringency	Primers must have at least 4 mismatches with unintended targets, including at least 2 mismatches within the last 4 bps at the 3' end
Primer Parameters	Primer size: 18-25 base pairs
	Primer GC content (%): 20-70
	Max Poly-X: 3
	Max GC in primer 3' end: 3

A primer optimization procedure was performed to select the best primers and temperature. Specifically, each primer was diluted to 10 pmol/µl, and cDNA samples were diluted 1+99 in dH_2O, and then different temperature grids were established by adding samples with or without cDNA to select the optimal annealing temperature. After identifying the gene of interest, qRT-PCR was performed. Each reaction consists of cDNA, IQ SYBR Green Supermix (Bio-Rad), and target-specific primers. Reactions were performed on a CFX Connect Real-Time PCR instrument (Bio-Rad, Copenhagen, Denmark). (Table VI)

Table VI. List of primers used in the two studies

Gene symbol	Forward primer sequence	Reverse primer sequence	Annealing temperature
ACTA2	5′-AGC AGC CCA GCC AAG CAC TG-3'	5′-AGC CGG CCT TAC AGA GCC CA-3′	60°C
SMTN	5'-CGC-GTG-TCT-AAT-CCG-TCG-GT-3'	5'-CGT-CGG-TTC-CTT-TCT-GGT-GA-3'	60°C
CNN1	5'-GTT-CGG-AGA-GGA-GAG-GCA-AA-3'	5'-AGG-CCG-TCC-ATG-AAG-TTG-TT-3'	60°C
CALD1	5'-TCT-GAG-CCT-TCT-GGT-3'	5'-CCT-CGG-GAA-GAA-GTT-3'	60°C
MYH11	5'-TGC-TTC-AAG-ATC-GGG-AGG-AC-3'	5'-GGC-CTT-GCG-TGA-TAC-TTG-TG-3'	60°C
COL1A1	5'-CCT-GGA-TGC-CAA-AGT-CT-3′	5'-AAT-CCA-TCG-GTC-ATG-CTC-TC-3′	62°C
ELN	5'-AAG-CAG-CAG-CAA-AGT-TCG-GT-3′	5'-ACT-AAG-CCT-GCA-GCA-GCT-CCA-TA-3′	62°C
PPIA	5'-TCC-TGG-CAT-CTT-GTC- CAT-G-3'	5'-CCA-TCC-AAC-CAC-TCA-GTC-TTG-3'	60°C
YWHAZ	5'-ACT-TTT-GGT-ACA-TTG-TGG-CTT-CAA-3'	5'-CCG-CCA-GGA-CAA-ACC-AGT-AT-3'	60°C
GAPDH	5'-ATG-CCT-CCT-GCA-CCA-CCA-ACT-3'	5'-ATG-GCA-TGG-ACT-GTG-GTC-ATG-AGT-3'	60°C

CHAPTER 5. SUMMARY OF THE RESULTS

Detailed results are described in each manuscript (Appendix II-III). In this section a brief overview of the main findings will be given.

5.1. First hypothesis

In vitro bioprinting of a stable 3D urethral smooth muscle model with high cell survival and induction of smooth muscle differentiation towards a contractile phenotype was possible using a hydrogel blend consisting of 7.5% (w/v) GelMA-3% (w/v) alginate.

To develop an *in vitro* 3D model that simulates the structure of the urethra, in the initial stages of the PhD project the current status of cell sources and manipulation approaches for application in urethral tissue engineering was reviewed (Appendix I). The comparison, as well as experimental results described in section 4.1, showed that smooth muscle cells have more advantages than adipose-derived stem cells in terms of culture time and differentiation degree.

Four different hydrogel formulations were prepared by combining different proportions (%w/v) of GelMA and alginate: G1 (5/1.5), G2 (5/3), G3 (7.5/1.5), and G4 (7.5/1.5). 10% GelMA served as the control group. Circular constructs were fabricated using an extrusion-based bio-printer with human bladder SMCs to mimic the circumferential smooth muscle layer of the urethra. First, rheological studies were performed on the hydrogels to understand their basic behavior. (Appendix II Figure 1). The results showed that at a constant printing temperature the viscosity of the hydrogel increased when the concentrations of GelMA and alginate were increased. When the temperature sweep was gradually lowered from 37 °C to the gel temperature range (20-30 °C), each group of hydrogels became stiffer. Pure GelMA solution (10%) showed a sol-gel transition rapidly at a narrow temperature range and reached the gel point faster.

All of blend hydrogels were able to maintain a stable gel state during the 3D printing process, which considerably reduced the limitations of pure GelMA in regard to its sensitivity to the temperature fluctuations. This was demonstrated by scanning at printing temperature and cooling temperature. It was demonstrated by examining the mechanical properties of each group of hydrogels after curing that, given the identical cross-linking procedure and time, the various concentrations of hydrogel polymers were responsible for the variations in each group's mechanical properties (Appendix II Figure 2). Analysis of the geometry and printing precision of the structures created from each set of hydrogels after 3D printing revealed that 7.5% GelMA-3% alginate had superior structural fidelity (Appendix II Figure 3).

Regarding cell viability, SMCs cultured in each of the five hydrogel groups had viability greater than 75% in the first two days after printing, indicating that the printing process had little effect on cell viability. The high cell viability was still present in each group on day 7 after printing, showing that the SMCs were able to achieve normal cell spreading and proliferation in the constructs in each group (Appendix II Figure 4). The mixed G3 and G4 hydrogels had higher proliferation rates, as shown by a comparison of cell proliferation rates (Appendix II Table II).

PCR was used to further assess the degree of SMC differentiation in each group of hydrogels seven days after the switch from growth medium to differentiation medium. Compared to the other hydrogel components, G4 likely provided the optimal environment to promote smooth muscle development towards a contractile phenotype and extracellular matrix (Appendix II Figures 4-6). Quantitative analysis by immunofluorescence and images showed that G4 presented a higher mean cellular fluorescence intensity for both SMA and MHC. The aspect ratio of the nuclei confirmed that G4 contained more elongated smooth muscle cells.

These findings imply that this approach may offer a feasible bioprinting platform for investigating smooth muscle phenotypic adaptation in three dimensions and that 7.5% GelMA-3% alginate may be a candidate hydrogel combination for bioprinting tissue engineered SMC constructs relevant for studying urethral regeneration.

5.2. Second hypothesis

Bioprinted bladder smooth muscle constructs subjected to cyclic mechanical stimulation exhibit improved contractile characteristics via p38 activation.

In study II, utilizing the optimal GelMA-alginate hybrid hydrogel combination developed in study I, we created an *in vitro* model to examine the impact of cyclic strain on bladder SMCs and the mechanism underlying this effect. Low adhesion commercially available plates were tailored to support adhesion of the hydrogels for application of cyclic strain to 3D printed cell constructs.

The degree of cell differentiation was examined by PCR and immunofluorescence. The results of PCR showed that all smooth muscle contraction-related markers were expressed to a higher extent in the cells of the four experimental groups than in the SMCs of the control group (cultured for 7 days in GM) after 6 days of differentiation and culture. Five differentiation markers showed significantly higher expression levels in the strain group compared with the other three experimental groups. The additional inhibitor concentration was inversely related to the differentiation level in both inhibitor groups. For the five markers, the group with the high concentration of inhibitor (Sb20) showed similar differentiation to the static group. This shows that the effects of mechanical stimulation on cells are almost neutralized by the p38 inhibitor at a concentration of 20 µM. (Appendix III Figure 2)

Immunofluorescence staining was used to identify the smooth muscle-specific contractile

proteins α-SMA and MHC to further evaluate the ability of the SMC-loaded constructs to differentiate under varied growth conditions. Figure 3 in Appendix III illustrates how smooth muscle cells varied in their expression levels of certain markers under various culture conditions. Consistent with RT-qPCR, it was discovered that cells in the strain group had significantly enhanced expression of α-SMA and MHC than those in the static group. The immunofluorescence intensity of cells in the constructs under strain with low quantities of inhibitor was also noticeably higher than that in the high concentration inhibitor group when comparing the effects of cyclic stretching in the presence of various amounts of inhibitor. Quantitative analysis of IF images (Appendix III Figure 4) and confocal microscopy images (Appendix III Figure 5) all showed similar results.

Study II showed that mechanical cycling stimulation promoted smooth muscle cell differentiation in 3D structures, and this effect was mediated through activation of the p38 pathway. Our results provide evidence for the differentiation of bladder smooth muscle cells in 3D, which may serve as a rationale for further mechanical stimulation. The results of this work are critical for a better understanding of how mechanical signals from the microenvironment are essential for maintaining the contractile phenotype of SMCs.

CHAPTER 6. GENERAL DISCUSSION

6.1. Choice of components for the bioink

In developing the optimal bioink, the first step was to consider the individual components of the bioink: the hydrogel, the photoinitiator, and the cell type. The hydrogel components selected were those previously shown to be capable of forming high-resolution tissue-like structures and promoting cell proliferation and differentiation [158]. GelMA hydrogels were initially selected for their excellent biocompatibility, photo-crosslinking, and adaptable physicochemical properties [159]. However, the high GelMA concentrations required to maintain structural fidelity had a detrimental effect, likely by reducing swelling and narrowing pore size, which restricted the diffusion of oxygen and nutrients required for cell survival, resulting in poor cell viability [148]. In addition, the highly temperature-sensitive rheological behavior of GelMA further limited its stability and consistency [160].

The strategy to solve these problems was to add alginate to increase the viscosity of the hydrogel. This approach offered the possibility to create constructs with high shape fidelity after crosslinking and to form stable filaments during the printing process. In addition, the choice of photoinitiator was also a focus, particularly with respect to the wavelength of light that must be used to crosslink the bioink. Several studies have shown that ultraviolet radiation may damage the DNA of cells, and depending of the dose it may lead to cell death, genomic mutations, or carcinogenesis. Therefore, when comparing the options of the bioprinter used in this study (Cellink, BIO X), the light source with a wavelength of 405 nm was preferred to that with 365 nm.

Compared to conventional photoinitiators (e.g., Irgacure 2959), LAP is more suitable for biological applications due to its excellent water solubility, cytocompatibility and other properties. Moreover, its absorption at 400 nm enables cross-linking at 405 nm UV light [161]. Finally, regarding the cell type, based on the structural and functional requirements for urethral regeneration, smooth muscle cells and adipose-derived stem cells were initially selected as candidate cells. By further comparing the differentiation ability and experimental duration in conjunction with the practical requirements of the experimental model, smooth muscle cells were finally selected as the cellular choice for this experiment.

6.2. Characterization of bioinks

To address the shortcomings of GelMA, a hybrid hydrogel containing alginate was investigated. Based on previous study on the range of application of the two concentrations of hydrogels, a series of experimental groups were prepared with in different ratios [125]. When the rheological properties were tested (Manuscript 2, Figure 1b), it was found that alginate helped to reduce the interaction between gelatin chains and the thermal behavior of GelMA. This meant that GelMA/alginate hybrid bioinks could better adapt to the printing environment where temperatures usually change. And due to the high loss modulus of alginate, it appeared to be viscoelastic and maintain a range of viscosities, making it easier to control rheology during the printing process.

6.3. Printing optimization of bioinks

To optimize the printing process, the cooling time of the mixed hydrogels after removal from the incubator was first adjusted to the different properties of the different hydrogel groups. Finally, it was found that the hydrogel groups were essentially viscoelastic solutions at a printing temperature of 28 °C, and this low viscosity state promoted continuous printing of the bioink and could effectively prevent clogging.

Additionally, it was discovered that the accuracy of the printed structures was directly correlated with the concentration of GelMA and alginate when comparing the printability of the hydrogels in each group. The findings here were in line with previous reports in the literature [162], which found that printability decreased with decreasing final polymer concentration in a GelMA/alginate mixture. It's important to remember that printability can still be improved even with G5's higher GelMA concentration. Additional factors that can be improved include curing time and photoinitiator concentration. Alginate was added to the G3 and G4 groups in this experiment, enhancing their capacity to print in the same printing environment and yielding extremely accurate and stable printable structures at low GelMA levels. This might be because, following UV crosslinking, the ionic crosslinking of Ca^{2+} increased the mechanical strength even further. GelMA and alginate final concentrations should be larger than 11%, according to earlier research, to construct 3D structures with stable geometries [162]. However, in our research, highly precise and printable structures could still be made for your top at final concentrations below 11%. This was due to the temperature-adjustable printing platform on the BIO-X bioprinter we employed, which, by lowering the printing platform's temperature, can help the newly created 3D constructions maintain a stable morphology and avoid collapsing in the first place.

High shear pressure in extrusion-based bioprinting has a significant impact on cell viability, according to earlier study [163]. Therefore, to maximize cell viability while guaranteeing that the hydrogel could be printed continuously, the size of the printing nozzle, printing pressure, speed, and curing time were all optimized. Another factor that lowers cell viability is exposure to UV radiation, particularly when cells are exposed to long periods of low wavelength UV light (385 nm) [164]. Here, the constructions were cross-linked for 15 seconds at 405 nm visible near-UV light. Since studies had demonstrated that after photocuring the cell-loaded structures with near-UV light for one minute or more, the viability and DNA integrity of MSCs remain unaltered [165].

6.4. Characterization of the 3D construct's mechanical performance

Characterization of the mechanical properties of the hydrogels after curing revealed that the hybrid hydrogels increased in crosslink density with increasing GelMA concentration, thus increasing stiffness. Whereas a certain range of stiffness is a key factor in maintaining cell spreading and further differentiation as the scaffold is porous, too much stiffness tends to reduce porosity, which further limits cell maturation and exchange with oxygen and nutrients. In turn, the different experimental groups exhibit different mechanical properties also leading to different biological behavior of the scaffolds. In this respect, G4 hydrogels seemed to offer a more suitable setting for SMC survival and development. These findings

were in line with earlier research that demonstrated how mechanical scaffold characteristics have a major impact on cell function, including attachment, spreading, and migration [166].

6.5. Characterization of scaffold's biological performance (viability, proliferation, differentiation)

The results of the live/dead assays on the day of printing and the next day of cell culture showed that all groups of seeded scaffolds had high cell viability, indicating that the printing process did not have a significant impact on cell viability, which was achieved by various factors optimized during the printing process.

Assessment of proliferation showed that cells proliferated in all groups. These cells were encapsulated in different concentrations of Bioink and still showed a tendency to proliferate on day 8. When comparing the proliferation rates, it was found that the cells proliferated faster in G3 and G4 hydrogels. This could be due to the different crosslink density of the hydrogels. G5 with the highest GelMA concentration tended to have stiffer mechanical properties after curing. And hydrogels that are too stiff may limit cell migration. And although G1 and G2 had lower GelMA concentrations, an evaluation of the mechanical properties showed that the stiffness of the scaffolds in the first four groups was very similar at the specific curing settings we used.

According to an analysis of the cells' capacity to differentiate in various conditions, G4 seems to be more favorable supporting the contractile phenotype of SMCs. Given that nuclear shape is a reliable parameter for assessing the SMC phenotype [167], and in response to morphological characterization of fluorescent photographs of cells, the fact that G4 induces elongated nuclear morphology is also evidence for differentiation of cells towards a contractile phenotype. These findings further the body of evidence indicating that the stiffness of smooth muscle can be maintained within a certain range while still maintaining its contractile nature [168–170]. Previous research has demonstrated that a soft growth environment encourages smooth muscle cells to change into a contractile phenotype, and that excessive mechanical stiffness inhibits the synthesis of a contractile SMC phenotype and instead encourages the growth of smooth muscle cells with a synthetic phenotype [167,171]. All genes related to SMC contractility were shown to be considerably increased in all experimental groups, with G4 cells showing the highest level of upregulation. The same findings were also found for the gene for the ECM-associated protein elastin. The transcriptional activity of collagen I, however, significantly increased in all groups following the initial 7-day induction period. This is consistent with previous research by Kindy indicating that collagen I expression would be increased in SMC cultures when exposed to reduced FBS and heparin [172]. This ECM protein may not react to changes in the composition of the hydrogel because the biochemical signal may be stronger than the mechanical signal, which could be an explanation. Overall, this study's findings show that matrix stiffness is a crucial factor in regulating maturation [173].

6.6. Surface modification of PDMS

Due to the hydrophobicity of the surface, the hydrogel's adherence to a commercially available Bioflex plate was insufficient for the trials. To boost the hydrophilicity of the Bioflex plates' untreated PDMS surface, we initially plasma-treated it. The method of choice was a water vapor/oxygen-based plasma treatment, and it has been demonstrated that functionalizing -OH groups can produce stable hydrophilic PDMS surfaces [174]. Following plasma treatment, two distinct approaches to combining the hybrid hydrogel with the hydrophilic PDMS surface in combination with the makeup of our experimental hybrid hydrogel were studied. To assist the cross-linking of PDMS with the GelMA component during UV curing, the first way includes adding methyl groups to the PDMS surface. TMSPMA, which includes a terminal methacrylate group that encourages strong covalent bonding with the acrylate group in the hydrogel under UV irradiation, is frequently employed to improve the adherence of hydrogels containing acrylate groups to hard surfaces [175,176]. To prevent cytotoxicity and damage to Bioflex plates among the several solvents previously used for TMSPMA, ethanol (99% v/v) was used [177–179]. It was discovered that the methyl-PDMS treatment preserved the adherence of the hydrogel to the Bioflex plate surface through testing in static and dynamic situations simulating experimental conditions. The hydrogel can be bound to the surface in situ while the bioprinted structure is being UV-cured, which speeds up the production process. This is another advantage of employing methyl-PDMS.

The addition of amino groups to the PDMS surface is a second method that relies on the covalent bonding of the alginate component to the PDMS by amide coupling between the amino group and the alginate's carboxylic acid group, which is facilitated by a carbodiimide [155]. The amino alteration failed to keep the constructions on the PDMS under static or dynamic settings, even though the majority of them stayed attached for a brief initial period of time. As opposed to this, a prior investigation by Cha and colleagues discovered that this method could effectively retain the adherence of alginate hydrogels to PDMS under mechanical loading (1 Hz, 10% strain) [155]. The inconsistency may be caused by the short crosslinking duration used in this investigation, whose authors used a 24-hour CaCl2 incubation. The key justification for the brief crosslinking period was to prevent maintaining the cells in CaCl2, which would have drastically decreased cell viability. Additionally, their technique relies on curing the alginate hydrogel and layer, which serves as a "glue" on the PDMS surface, concurrently. Because the print head cannot establish a normal geometry on an uneven hydrogel pre-solution surface, this technology is unable to meet our 3D bioprinting criteria. Therefore, we chose to print on a surface already coated with the curing 'glue' - alginate - to finalize the curing of the blend bioinks.

6.7. The role of cyclic strain on 3D constructs

The constructs were stamped in the center of the well, where isometric strain fields appeared to be more homogeneous according to empirical research and finite element modeling [180]. Although the membrane was subjected to a maximum nominal strain of 5%, it was discovered that the actual strain in the hydrogel was closer to 4.3%. The rigidity of the hydrogel and PDMS membranes may be the cause of this discrepancy. However, in this work, the relationship between nominal and actual strain appeared to follow a linear

relationship along the entire range of interest. In the past, it was suggested that the mechanical mismatch between PDMS and hydrogel could cause a non-linearity between the applied strain and the actual strain, particularly for low strain values.

In the past, uniaxial loading stimulation of vascular SMCs had been used to study the effects of mechanical stimulation on SMCs inside of three-dimensional stents [181]. Uniaxial forces acting on the vascular wall were mostly to blame for this. Even Nevertheless, it seems more logical to utilize biaxial strain while researching bladder SMCs because the bladder wall is prone to multi-axial stresses during filling and emptying [182]. When it came to the activation of internal molecular processes and cytoskeletal reorganization, cells would be able to recognize distinctions between uniaxial and isometric loading. In both 2D and 3D configurations, uniaxial stress often caused SMC cell migration and cytoskeletal reorganization [181,183–185]. Skeletal muscle cells, for instance, react differently to mechanical stimuli depending on the orientation [180,186]. The paradigm used here, it was hypothesized, would more accurately depict the physiological strain field of the bladder wall. In keeping with this, Chae and colleagues created an *in vitro* bladder model using bioprinted bone marrow-derived stem cells (BMSCs) that were stimulated mechanically under isometric strain to simulate the stresses on the cells *in vivo* [142].

The findings of this study unambiguously showed that SMCs respond to cyclic mechanical stimulation by displaying morphological alterations, a gradual rise in gene transcription, and higher expression of contractile marker proteins, all of which were connected to a contractile phenotype. This is in accordance with a recent study [142]that found cyclic mechanical stimulation of 3D constructions increased BMSC development towards the smooth muscle lineage. Additionally, it was discovered that the effects of mechanical stimulation were eliminated by the maximum dose of p38 inhibitor (20 µm), indicating that the p38 MAPK pathway is crucial in regulating the differentiation of bladder SMCs in response to mechanical stimulation. It may not come as a surprise that p38 inhibitors have an impact on mechanical reactions given that this MAPK plays a general role in the transmission of multiple signaling pathways, including diverse ligands and stressors [187]. Cyclical stress caused SMCs to produce more cytoskeletal and contractile domain proteins as well as microfilaments, all of which were suppressed by p38 inhibitors [188]. Like this, *in vitro* investigations using two-dimensional bladder SMCs had shown that p38 MAPK plays a role in translating mechanical inputs into differentiation signals [142,144,189].

What is unique about study II is that it focuses on the creation of a 3D model, as most previous *in vitro* studies on the effects of cyclic loading on SMCs have been based on a flexible 2D culture substrate. Another unique feature was the introduction of an equiaxial strain field into the 3D construct, as previous studies have focused on uniaxial loading relevant to airway or vascular SMCs, but not visceral SMCs.

6.8. Limitations and further work

One of the limitations of this work was that only a finite number of hydrogel combinations could be prepared during the phase of developing the optimal hydrogel. Another limitation is that rheological and mechanical properties were studied on constructs without cells. Despite the use of a 1:10 ratio in the combination of cell culture and hydrogel, these small amounts of culture medium could have affected the rheological properties of the hydrogel during the printing process. As for the measurements of mechanical properties post-cross linking, measurements could have been in cell-loaded constructs at different times during the culture process to better visualize the changes in the mechanical properties of the hydrogel over time. Another limitation was the use of a relatively modest cell density ($2x10^6$ cells/ml) to better study cell spreading. A more accurate mimic of the smooth muscle layer could possibly have been achieved with a higher cell density. Since the purpose of this work was to show that smooth muscle cells are still viable after bioprinting, the experiments were performed for a limited period. However, it would be necessary to further investigate the long-term growth and maturation of the cells.

The results presented here are encouraging and will enable the use of these constructs as a platform for studying the mechanisms of phenotypic transformation of SMCs and for developing tissue engineering approaches for LUT. However, there are certain limitations. Strain greater than 5%, which has been commonly used in previous *in vitro* studies, has not been applied to SMCs. Strains of up to 20% have been used in research to study pathological situations (e.g., bladder outlet obstruction). Future research will show whether the approach described here can be applied to simulate such strains. In addition to the loading amplitude, other factors such as effective exposure time, cycle duration, and rest time could have a major impact on the outcome. Therefore, it might be necessary to better optimize the time-dependent effects of cyclic mechanical stimulation. Another drawback is that only adhesion to the hydrogel after PDMS modification was evaluated for a short period of time to match the experimental design (i.e., 7 days of cell growth under static conditions, 6 days of cell differentiation, and 1 h/day of cyclic mechanical stimulation). Therefore, further studies on the experimental setup and test cycle are needed to confirm the robustness of the method.

CHAPTER 7. CONCLUSIONS

In this work, it was shown that a blend hydrogel comprising GelMA and alginate allowed bioprinting of consistent SMC structures that could be bioprinted while maintaining high cell viability. The results showed that G4 (7.5/3 w/v %) exhibited higher structural fidelity and supported a more contractile SMC phenotype of the printed cells. The use of alginate helped to reduce the limitations of GelMA in terms of temperature sensitivity while maintaining the advantages of low-concentration GelMA in terms of cytocompatibility. It was evident that the mechanical properties of the hydrogels were critical for triggering the contractile phenotype of SMCs. Custom modifications to commercially available culture plates enabled the application of cyclic mechanical stimuli to the bioprinted 3D constructs. According to the results, activation of p38 MAPK is the mechanism by which cyclic mechanical loading causes the transformation of cultured bladder SMCs to a contractile phenotype.

The results of this work contribute to a better understanding of how mechanical cues from the 3D microenvironment maintain the contractile phenotype of SMCs. The approach developed here may provide a useful 3D platform for exploring the phenotypic adaptability of smooth muscle and could have significant implications for the development of new therapies for urethral strictures.

REFFERENCES

1. Hampson LA, McAninch JW, Breyer BN. Male urethral strictures and their management. Nat Rev Urol 2014;11(1):43–50; doi: 10.1038/nrurol.2013.275.
2. Jordan GH. Principles of tissue transfer techniques in urethral reconstruction. Urologic Clinics of North America 2002;29(2):267–275; doi: 10.1016/S0094-0143(02)00034-4.
3. Dublin N, Stewart LH. Oral complications after buccal mucosal graft harvest for urethroplasty. BJU Int 2004;94(6):867–869; doi: 10.1111/j.1464-410X.2004.05048.x.
4. Goldfarb DA. Tissue Engineering Stem Cells, and Cloning: Opportunities for Regenerative Medicine. Journal of Urology 2005;(173(4)):1431–1432.
5. Osman NI, Hillary C, Bullock AJ, et al. Tissue engineered buccal mucosa for urethroplasty: Progress and future directions. Adv Drug Deliv Rev 2015;82:69–76; doi: 10.1016/j.addr.2014.10.006.
6. Chan YY, Bury MI, Yura EM, et al. The current state of tissue engineering in the management of hypospadias. Nat Rev Urol 2020;17(3):162–175; doi: 10.1038/s41585-020-0281-4.
7. Sharma AK, Cheng EY. Growth factor and small molecule influence on urological tissue regeneration utilizing cell seeded scaffolds. Adv Drug Deliv Rev 2015;82:86–92; doi: 10.1016/j.addr.2014.11.008.
8. Damaser MS, Sievert KD. Tissue engineering and regenerative medicine: Bench to bedside in urology. Adv Drug Deliv Rev 2015;82:v–vii; doi: 10.1016/j.addr.2015.01.006.
9. Mantha S, Pillai S, Khayambashi P, et al. Smart Hydrogels in Tissue Engineering and. Materials 2019;12(3323):33.
10. Zhang K, Fu Q, Yoo J, et al. 3D bioprinting of urethra with PCL/PLCL blend and dual autologous cells in fibrin hydrogel: An in vitro evaluation of biomimetic mechanical property and cell growth environment. Acta Biomater 2017;50:154–164; doi: 10.1016/j.actbio.2016.12.008.
11. Lee CH, Akin-Olugbade O, Kirschenbaum A. Overview of Prostate Anatomy, Histology, and Pathology. Endocrinol Metab Clin North Am 2011;40(3):565–575; doi: 10.1016/j.ecl.2011.05.012.
12. Amjad Alwaal , Sarah D Blaschko , Jack W McAninch BNB. Epidemiology of urethral strictures. Transl Androl Urol 2014;3(2):209–213; doi: 10.3978/j.issn.2223-4683.2014.04.07.
13. Pal D, Kumar S, Ghosh B. Direct visual internal urethrotomy: Is it a durable treatment option? Urol Ann 2017;9(1):18–22; doi: 10.4103/0974-7796.198835.
14. Launonen E, Sairanen J, Ruutu M, et al. Role of visual internal urethrotomy in pediatric urethral strictures. J Pediatr Urol 2014;10(3):545–549; doi: 10.1016/j.jpurol.2013.11.018.
15. Wong SS, Aboumarzouk OM, Narahari R, et al. Simple urethral dilatation, endoscopic urethrotomy, and urethroplasty for urethral stricture disease in adult men. Cochrane Database of Systematic Reviews 2012; doi: 10.1002/14651858.cd006934.pub3.
16. Devine PC, Wendelken JR, Devine CJ. Free full thickness skin graft urethroplasty: Current technique. Journal of Urology 1979;121(3):282–285; doi: 10.1016/S0022-5347(17)56754-3.
17. Chapple C. Tissue engineering of the urethra: where are we in 2019? World J Urol 2019;(0123456789):1–5; doi: 10.1007/s00345-019-02826-3.

18. Bhargava S, Chapple CR. Buccal mucosal urethroplasty: Is it the new gold standard? BJU Int 2004;93(9):1191–1193; doi: 10.1111/j.1464-410X.2003.04860.x.
19. Spilotros M, Sihra N, Malde S, et al. Buccal mucosal graft urethroplasty in men-risk factors for recurrence and complications: A third referral centre experience in anterior urethroplasty using buccal mucosal graft. Transl Androl Urol 2017;6(3):510–516; doi: 10.21037/tau.2017.03.69.
20. Sergeant GP, Hollywood MA, Thornbury KD. Spontaneous Activity in Urethral Smooth Muscle. Adv Exp Med Biol 2019;1124:149–167; doi: 10.1007/978-981-13-5895-1_6.
21. Fry CH, Meng E, Young JS. The physiological function of lower urinary tract smooth muscle. Auton Neurosci 2010;154(1–2):3–13; doi: 10.1016/j.autneu.2009.10.006.
22. Abbas TO, Yalcin HC, Pennisi CP. From Acellular Matrices to Smart Polymers: Degradable Scaffolds that are Transforming the Shape of Urethral Tissue Engineering. Int J Mol Sci 2019;20(7):1763; doi: 10.3390/ijms20071763.
23. Gordon D, Reidy MA, Benditt EP, et al. Cell proliferation in human coronary arteries. Proc Natl Acad Sci U S A 1990;87(12):4600–4604; doi: 10.1073/pnas.87.12.4600.
24. Beamish JA, He P, Kottke-Marchant K, et al. Molecular regulation of contractile smooth muscle cell phenotype: Implications for vascular tissue engineering. Tissue Eng Part B Rev 2010;16(5):467–491; doi: 10.1089/ten.teb.2009.0630.
25. Xue JD, Gao J, Fu Q, et al. Seeding cell approach for tissue-engineered urethral reconstruction in animal study: A systematic review and meta-analysis. Exp Biol Med 2016;241(13):1416–1428; doi: 10.1177/1535370216640148.
26. Mangir N, Wilson KJ, Osman NI, et al. Current state of urethral tissue engineering. Curr Opin Urol 2019;29(4):385–393; doi: 10.1097/MOU.0000000000000637.
27. Chen Q, Zhu L, Zhao C, et al. A robust, one-pot synthesis of highly mechanical and recoverable double network hydrogels using thermoreversible sol-gel polysaccharide. Advanced Materials 2013;25(30):4171–4176; doi: 10.1002/adma.201300817.
28. Li X, Wang H, Li D, et al. Dual Ionically Cross-linked Double-Network Hydrogels with High Strength, Toughness, Swelling Resistance, and Improved 3D Printing Processability. ACS Appl Mater Interfaces 2018;10(37):31198–31207; doi: 10.1021/acsami.8b13038.
29. Naahidi S, Jafari M, Logan M, et al. Biocompatibility of hydrogel-based scaffolds for tissue engineering applications. Biotechnol Adv 2017;35(5):530–544; doi: 10.1016/j.biotechadv.2017.05.006.
30. Yang J, Zhang YS, Yue K, et al. Cell-laden hydrogels for osteochondral and cartilage tissue engineering. Acta Biomater 2017;57:1–25; doi: 10.1016/j.actbio.2017.01.036.
31. Caneparo C, Brownell D, Chabaud S, et al. Genitourinary tissue engineering: Reconstruction and research models. Bioengineering 2021;8(7); doi: 10.3390/bioengineering8070099.
32. Rashidbenam Z, Jasman MH, Hafez P, et al. Overview of Urethral Reconstruction by Tissue Engineering: Current Strategies, Clinical Status and Future Direction. Tissue Eng Regen Med 2019;16(4):365–384; doi: 10.1007/s13770-019-00193-z.
33. Sayeg K, Freitas-Filho LG, Waitzberg ÂFL, et al. Integration of collagen matrices into the urethra when implanted as onlay graft. International Braz J

Urol 2013;39(3):414–423; doi: 10.1590/S1677-5538.IBJU.2013.03.16.
34. Micol LA, Arenas da Silva LF, Geutjes PJ, et al. In-vivo performance of high-density collagen gel tubes for urethral regeneration in a rabbit model. Biomaterials 2012;33(30):7447–7455; doi: 10.1016/j.biomaterials.2012.06.087.
35. Pinnagoda K, Larsson HM, Vythilingam G, et al. Engineered acellular collagen scaffold for endogenous cell guidance, a novel approach in urethral regeneration. Acta Biomater 2016;43:208–217; doi: 10.1016/j.actbio.2016.07.033.
36. Tachibana M, Nagamatsu GR, Addonizio JC. Ureteral replacement using collagen sponge tube grafts. Journal of Urology 1985;133(5):866–869; doi: 10.1016/S0022-5347(17)49268-8.
37. Larsson HM, Vythilingam G, Pinnagoda K, et al. Fiber density of collagen grafts impacts rabbit urethral regeneration. Sci Rep 2018;8(1):1–8; doi: 10.1038/s41598-018-27621-9.
38. Sartoneva R, Haaparanta AM, Lahdes-Vasama T, et al. Characterizing and optimizing poly-L-lactide-co-1-caprolactone membranes for urothelial tissue engineering. J R Soc Interface 2012;9(77):3444–3454; doi: 10.1098/rsif.2012.0458.
39. Hu J, Ai B, Zhu S, et al. Electrospun PLGA and PLGA/gelatin scaffolds for tubularized urethral replacement: Studies in vitro and in vivo. J Biomater Appl 2022;36(6):956–964; doi: 10.1177/08853282211030904.
40. Liu G, Fu M, Li F, et al. Tissue-engineered PLLA/gelatine nanofibrous scaffold promoting the phenotypic expression of epithelial and smooth muscle cells for urethral reconstruction. Materials Science and Engineering C 2020;111(March):110810; doi: 10.1016/j.msec.2020.110810.
41. Fu WJ, Wang ZX, Li G, et al. A surface-modified biodegradable urethral scaffold seeded with urethral epithelial cells. Chin Med J (Engl) 2011;124(19):3087–3092; doi: 10.3760/cma.j.issn.0366-6999.2011.19.025.
42. Niu Y, Galluzzi M, Deng F, et al. A biomimetic hyaluronic acid-silk fibroin nanofiber scaffold promoting regeneration of transected urothelium. Bioeng Transl Med 2022;7(2):1–13; doi: 10.1002/btm2.10268.
43. Algarrahi K, Affas S, Sack BS, et al. Repair of injured urethras with silk fibroin scaffolds in a rabbit model of onlay urethroplasty. Journal of Surgical Research 2018;229:192–199; doi: 10.1016/j.jss.2018.04.006.
44. Xie M, Song L, Wang J, et al. Evaluation of stretched electrospun silk fibroin matrices seeded with urothelial cells for urethra reconstruction. Journal of Surgical Research 2013;184(2):774–781; doi: 10.1016/j.jss.2013.04.016.
45. Lv XG, Li Z, Chen SY, et al. Structural and functional evaluation of oxygenating keratin/silk fibroin scaffold and initial assessment of their potential for urethral tissue engineering. Biomaterials 2016;84:99–110; doi: 10.1016/j.biomaterials.2016.01.032.
46. Chung YG, Tu D, Franck D, et al. Acellular bi-layer silk fibroin scaffolds support tissue regeneration in a rabbit model of onlay urethroplasty. PLoS One 2014;9(3):1–7; doi: 10.1371/journal.pone.0091592.
47. Xie M, Xu Y, Song L, et al. Tissue-engineered buccal mucosa using silk fibroin matrices for urethral reconstruction in a canine model. Journal of Surgical Research 2014;188(1):1–7; doi: 10.1016/j.jss.2013.11.1102.
48. Naji M, Rasouli J, Shakhssalim N, et al. Supportive features of a new hybrid scaffold for urothelium engineering. Archives of Medical Science 2015;11(2):438–445; doi: 10.5114/aoms.2015.50977.
49. Klekiel T, Mackiewicz A, Kaczmarek-Pawelska A, et al. Novel design of sodium alginate based absorbable stent for the use in urethral stricture disease.

Journal of Materials Research and Technology 2020;9(4):9004–9015; doi: 10.1016/j.jmrt.2020.06.047.
50. Lv X, Guo Q, Han F, et al. Electrospun poly(L-lactide)/poly(ethylene glycol) scaffolds seeded with human amniotic mesenchymal stem cells for urethral epithelium repair. Int J Mol Sci 2016;17(8); doi: 10.3390/ijms17081262.
51. Niu Y, Stadler FJ, Yang X, et al. HA-coated collagen nanofibers for urethral regeneration via in situ polarization of M2 macrophages. J Nanobiotechnology 2021;19(1):1–14; doi: 10.1186/s12951-021-01000-5.
52. Huang JW, Lv XG, Li Z, et al. Urethral reconstruction with a 3D porous bacterial cellulose scaffold seeded with lingual keratinocytes in a rabbit model. Biomedical Materials (Bristol) 2015;10(5); doi: 10.1088/1748-6041/10/5/055005.
53. Liu G, Fu M, Li F, et al. Tissue-engineered PLLA/gelatine nanofibrous scaffold promoting the phenotypic expression of epithelial and smooth muscle cells for urethral reconstruction. Materials Science and Engineering C 2020;111(March):110810; doi: 10.1016/j.msec.2020.110810.
54. Kajbafzadeh AM, Sabetkish S, Tourchi A, et al. The application of tissue-engineered preputial matrix and fibrin sealant for urethral reconstruction in rabbit model. Int Urol Nephrol 2014;46(8):1573–1580; doi: 10.1007/s11255-014-0684-3.
55. Kanatani I, Kanematsu A, Inatsugu Y, et al. Fabrication of an optimal urethral graft using collagen-sponge tubes reinforced with copoly(L-lactide/ε-caprolactone) fabric. Tissue Eng 2007;13(12):2933–2940; doi: 10.1089/ten.2007.0052.
56. Hongfeng Z, Changhong Q, Jun J, et al. Experimental study of tissue-engineered urethra with collagen / chitosan composite as scaffolds. 2020.
57. Wang DJ, Li MY, Huang WT, et al. Repair of urethral defects with polylactid acid fibrous membrane seeded with adipose-derived stem cells in a rabbit model. Connect Tissue Res 2015;56(6):434–439; doi: 10.3109/03008207.2015.1035376.
58. Rapoport HS, Fish J, Basu J, et al. Construction of a tubular scaffold that mimics j-shaped stress/strain mechanics using an innovative electrospinning technique. Tissue Eng Part C Methods 2012;18(8):567–574; doi: 10.1089/ten.tec.2011.0286.
59. Raya-Rivera A, Esquiliano DR, Yoo JJ, et al. Tissue-engineered autologous urethras for patients who need reconstruction: An observational study. The Lancet 2011;377(9772):1175–1182; doi: 10.1016/S0140-6736(10)62354-9.
60. Hu J, Ai B, Zhu S, et al. Electrospun PLGA and PLGA/gelatin scaffolds for tubularized urethral replacement: Studies in vitro and in vivo. J Biomater Appl 2022;36(6):956–964; doi: 10.1177/08853282211030904.
61. Gu X, Xu Y, Li S, et al. Preparation of a Photocured Biocompatible Hydrogel for Urethral Tissue Engineering. ACS Appl Polym Mater 2021;3(7):3519–3527; doi: 10.1021/acsapm.1c00427.
62. Murphy S v., Atala A. 3D bioprinting of tissues and organs. Nat Biotechnol 2014;32(8):773–785; doi: 10.1038/nbt.2958.
63. Ramsay S, Ringuette-Goulet C, Langlois A, et al. Clinical challenges in tissue-engineered urethral reconstruction. Transl Androl Urol 2016;5(2):267–270; doi: 10.21037/tau.2016.01.11.
64. Ayala R, Zhang C, Yang D, et al. Engineering the cell-material interface for controlling stem cell adhesion, migration, and differentiation. Biomaterials 2011;32(15):3700–3711; doi: 10.1016/j.biomaterials.2011.02.004.

65. Bajaj P, Schweller RM, Khademhosseini A, et al. 3D biofabrication strategies for tissue engineering and regenerative medicine. Annu Rev Biomed Eng 2014;16:247–276; doi: 10.1146/annurev-bioeng-071813-105155.
66. Drury JL, Mooney DJ. Hydrogels for tissue engineering: Scaffold design variables and applications. Biomaterials 2003;24(24):4337–4351; doi: 10.1016/S0142-9612(03)00340-5.
67. de Filippo RE, Yoo JJ, Atala A. Urethral replacement using cell seeded tubularized collagen matrices. Journal of Urology 2002;168(4 II):1789–1793; doi: 10.1097/00005392-200210020-00032.
68. Palminteri E, Berdondini E, Fusco F, et al. Long-term results of small intestinal submucosa graft in bulbar urethral reconstruction. Urology 2012;79(3):695–701; doi: 10.1016/j.urology.2011.09.055.
69. Versteegden LRM, de Jonge PKJD, IntHout J, et al. Tissue Engineering of the Urethra: A Systematic Review and Meta-analysis of Preclinical and Clinical Studies [Figure presented]. Eur Urol 2017;72(4):594–606; doi: 10.1016/j.eururo.2017.03.026.
70. Hickling DR, Sun TT, Wu XR. Anatomy and physiology of the urinary tract: Relation to host defense and microbial infection. Urinary Tract Infections: Molecular Pathogenesis and Clinical Management 2016;(3):3–25; doi: 10.1128/9781555817404.ch1.
71. Mangera A, Osman N, Chapple C. Evaluation and management of anterior urethral stricture disease. F1000Res 2016;5:1–6; doi: 10.12688/f1000research.7121.1.
72. Wang F, Liu T, Yang L, et al. Urethral reconstruction with tissue-engineered human amniotic scaffold in rabbit urethral injury models. Medical Science Monitor 2014;20:2430–2438; doi: 10.12659/MSM.891042.
73. Fossum M, Svensson J, Kratz G, et al. Autologous in vitro cultured urothelium in hypospadias repair{star, open}. J Pediatr Urol 2007;3(1):10–18; doi: 10.1016/j.jpurol.2006.01.018.
74. Giuseppe Romagnoli, Michele De Luca, Fabio Faranada, Roberto Bandelloni, Adriano Tito Franzi, Ferdinando Cataliotti RC. Treatment of posterior hypospadias by the autologous graft of cultured urethral epithelium. The New English Journal of medicine 1990;323(16):1120–1123.
75. Guido Barbagli, Arezzo, Italy; Gouya Ram Liebig D, Germany; Dirk Fahlenkamp, Chemnitz GML. New Bulbar Urethroplasty Using Tissue-Engineered Oral Mucosal Graft: a Preliminary Clinical Report. Journal of Urology 2013;189(4S):e1; doi: 10.1016/j.juro.2013.02.1376.
76. Oottamasathien S, Wang YQ, Williams K, et al. Directed differentiation of embryonic stem cells into bladder tissue. Dev Biol 2007;304(2):556–566; doi: 10.1016/j.ydbio.2007.01.010.
77. Mauney JR, Ramachandran A, Yu RN, et al. All-trans retinoic acid directs urothelial specification of murine embryonic stem cells via GATA4/6 signaling mechanisms. PLoS One 2010;5(7); doi: 10.1371/journal.pone.0011513.
78. Orabi H, Aboushwareb T, Zhang Y, et al. Cell-seeded tubularized scaffolds for reconstruction of long urethral defects: A preclinical study. Eur Urol 2013;63(3):531–538; doi: 10.1016/j.eururo.2012.07.041.
79. Feng C, Xu YM, Fu Q, et al. Reconstruction of three-dimensional neourethra using lingual keratinocytes and corporal smooth muscle cells seeded acellular corporal spongiosum. Tissue Eng Part A 2011;17(23–24):3011–3019; doi: 10.1089/ten.tea.2011.0061.
80. Osborn SL, Thangappan R, Luria A, et al. Induction of Human Embryonic and

Induced Pluripotent Stem Cells Into Urothelium. Stem Cells Transl Med 2014;3(5):610–619; doi: 10.5966/sctm.2013-0131.
81. Moad M, Pal D, Hepburn AC, et al. A novel model of urinary tract differentiation, tissue regeneration, and disease: Reprogramming human prostate and bladder cells into induced pluripotent stem cells. Eur Urol 2013;64(5):753–761; doi: 10.1016/j.eururo.2013.03.054.
82. Bhargava S, Patterson JM, Inman RD, et al. Tissue-Engineered Buccal Mucosa Urethroplasty-Clinical Outcomes. Eur Urol 2008;53(6):1263–1271; doi: 10.1016/j.eururo.2008.01.061.
83. Osman NI, Patterson JM, Macneil S, et al. Long-term follow-up after tissue-engineered buccal mucosa urethroplasty. Eur Urol 2014;66(4):790–791; doi: 10.1016/j.eururo.2014.07.007.
84. Tian H, Bharadwaj S, Liu Y, et al. Differentiation of human bone marrow mesenchymal stem cells into bladder cells: Potential for urological tissue engineering. Tissue Eng Part A 2010;16(5):1769–1779; doi: 10.1089/ten.tea.2009.0625.
85. Liu JS, Bury MI, Fuller NJ, et al. Bone Marrow Stem/Progenitor Cells Attenuate the Inflammatory Milieu Following Substitution Urethroplasty. Sci Rep 2016;6(October):4–10; doi: 10.1038/srep35638.
86. Fu Q, Deng CL, Liu W, et al. Urethral replacement using epidermal cell-seeded tubular acellular bladder collagen matrix. BJU Int 2007;99(5):1162–1165; doi: 10.1111/j.1464-410X.2006.06691.x.
87. Rogovaya OS, Fayzulin AK, Vasiliev A v., et al. Reconstruction of rabbit urethral epithelium with skin keratinocytes. Acta Naturae 2015;7(1):70–77; doi: 10.32607/20758251-2015-7-1-70-77.
88. Zhang M, Peng Y, Zhou Z, et al. Differentiation of human adipose-derived stem cells Co-cultured with urothelium cell line toward a urothelium-like phenotype in a nude murine model. Urology 2013;81(2):465.e15-465.e22; doi: 10.1016/j.urology.2012.10.030.
89. Gu GL, Xia SJ, Zhang J, et al. Tubularized urethral replacement using tissue-engineered peritoneum-like tissue in a rabbit model. Urol Int 2012;89(3):358–364; doi: 10.1159/000339745.
90. Zhang D, Wei G, Li P, et al. Urine-derived stem cells: A novel and versatile progenitor source for cell-based therapy and regenerative medicine. Genes Dis 2014;1(1):8–17; doi: 10.1016/j.gendis.2014.07.001.
91. Drewa T, Joachimiak R, Bajek A, et al. Hair follicle stem cells can be driven into a urothelial-like phenotype: An experimental study. International Journal of Urology 2013;20(5):537–542; doi: 10.1111/j.1442-2042.2012.03202.x.
92. Kang HH, Kang JJ, Kang HG, et al. Urothelial differentiation of human amniotic fluid stem cells by urothelium specific conditioned medium. Cell Biol Int 2014;38(4):531–537; doi: 10.1002/cbin.10232.
93. Lv X, Guo Q, Han F, Chen C, Ling C, Chen W, et al. Electrospun poly(l-lactide)/poly(ethylene glycol) scaffolds seeded with human amniotic mesenchymal stem cells for urethral epithelium repair. Int J Mol Sci. 2016;17:E1262. doi: 10.3390/ijms17081262.
94. Zhang M, Xu MX, Zhou Z, et al. The differentiation of human adipose-derived stem cells towards a urothelium-like phenotype in vitro and the dynamic temporal changes of related cytokines by both paracrine and autocrine signal regulation. PLoS One 2014;9(4); doi: 10.1371/journal.pone.0095583.
95. Liu J, Huang J, Lin T, et al. Cell-to-cell contact induces human adipose tissue-derived stromal cells to differentiate into urothelium-like cells in vitro. Biochem

Biophys Res Commun 2009;390(3):931–936; doi: 10.1016/j.bbrc.2009.10.080.
96. Zhang R, Jack GS, Rao N, et al. Nuclear fusion-independent smooth muscle differentiation of human adipose-derived stem cells induced by a smooth muscle environment. Stem Cells 2012;30(3):481–490; doi: 10.1002/stem.1023.
97. Fu Q, Deng CL, Zhao RY, et al. The effect of mechanical extension stimulation combined with epithelial cell sorting on outcomes of implanted tissue-engineered muscular urethras. Biomaterials 2014;35(1):105–112; doi: 10.1016/j.biomaterials.2013.09.067.
98. Riis S, Hansen AC, Johansen L, et al. Fabrication and characterization of extracellular matrix scaffolds obtained from adipose-derived stem cells. Methods 2020;171:68–76; doi: 10.1016/j.ymeth.2019.07.004.
99. Nakamura M, Iwanaga S, Henmi C, et al. Biomatrices and biomaterials for future developments of bioprinting and biofabrication. Biofabrication 2010;2(1); doi: 10.1088/1758-5082/2/1/014110.
100. Zhang B, Luo Y, Ma L, et al. 3D bioprinting: an emerging technology full of opportunities and challenges. Biodes Manuf 2018;1(1):2–13; doi: 10.1007/s42242-018-0004-3.
101. Bhardwaj N, Kundu SC. Electrospinning: A fascinating fiber fabrication technique. Biotechnol Adv 2010;28(3):325–347; doi: 10.1016/j.biotechadv.2010.01.004.
102. Zhang K, Guo X, Zhao W, et al. Application of Wnt pathway inhibitor delivering scaffold for inhibiting fibrosis in urethra strictures: In vitro and in vivo study. Int J Mol Sci 2015;16(11):27659–27676; doi: 10.3390/ijms161126050.
103. Li C, Xu YM, Liu ZS, et al. Urethral reconstruction with tissue engineering and RNA interference techniques in rabbits. Urology 2013;81(5):1075–1080; doi: 10.1016/j.urology.2013.01.041.
104. Niu Y, Galluzzi M, Deng F, et al. A biomimetic hyaluronic acid-silk fibroin nanofiber scaffold promoting regeneration of transected urothelium. Bioeng Transl Med 2022;7(2):1–13; doi: 10.1002/btm2.10268.
105. Guillotin B, Souquet A, Catros S, et al. Laser assisted bioprinting of engineered tissue with high cell density and microscale organization. Biomaterials 2010;31(28):7250–7256; doi: 10.1016/j.biomaterials.2010.05.055.
106. Dababneh AB, Ozbolat IT. Bioprinting Technology: A Current State-of-the-Art Review. Journal of Manufacturing Science and Engineering, Transactions of the ASME 2014;136(6):1–11; doi: 10.1115/1.4028512.
107. Wüst S, Müller R, Hofmann S. Controlled Positioning of Cells in Biomaterials—Approaches Towards 3D Tissue Printing. 2011.; doi: 10.3390/jfb2030119.
108. Saunders RE, Derby B. Inkjet printing biomaterials for tissue engineering: Bioprinting. International Materials Reviews 2014;59(8):430–448; doi: 10.1179/1743280414Y.0000000040.
109. Jana S, Lerman A. Bioprinting a cardiac valve. Biotechnol Adv 2015;33(8):1503–1521; doi: 10.1016/j.biotechadv.2015.07.006.
110. Lal H, Patralekh MK. 3D printing and its applications in orthopaedic trauma: A technological marvel. J Clin Orthop Trauma 2018;9(3):260–268; doi: 10.1016/j.jcot.2018.07.022.
111. Kyle S, Jessop ZM, Al-Sabah A, et al. 'Printability'' of Candidate Biomaterials for Extrusion Based 3D Printing: State-of-the-Art.' Adv Healthc Mater 2017;6(16):1–16; doi: 10.1002/adhm.201700264.
112. Ozbolat IT, Hospodiuk M. Current advances and future perspectives in extrusion-based bioprinting. Biomaterials 2016;76:321–343;

doi: 10.1016/j.biomaterials.2015.10.076.
113. Gungor-Ozkerim PS, Inci I, Zhang YS, et al. Bioinks for 3D bioprinting: An overview. Biomater Sci 2018;6(5):915–946; doi: 10.1039/c7bm00765e.
114. Ouyang L, Highley CB, Rodell CB, et al. 3D Printing of Shear-Thinning Hyaluronic Acid Hydrogels with Secondary Cross-Linking. ACS Biomater Sci Eng 2016;2(10):1743–1751; doi: 10.1021/acsbiomaterials.6b00158.
115. Choi YJ, Park H, Ha DH, et al. 3D bioprinting of in vitro models using hydrogel-based bioinks. Polymers (Basel) 2021;13(3):1–18; doi: 10.3390/polym13030366.
116. Mousavi SJ, Hamdy Doweidar M. Role of mechanical cues in cell differentiation and proliferation: A 3D numerical model. PLoS One 2015;10(5):1–23; doi: 10.1371/journal.pone.0124529.
117. Hsieh FY, Lin HH, Hsu S hui. 3D bioprinting of neural stem cell-laden thermoresponsive biodegradable polyurethane hydrogel and potential in central nervous system repair. Biomaterials 2015;71:48–57; doi: 10.1016/j.biomaterials.2015.08.028.
118. Hölzl K, Lin S, Tytgat L, et al. Bioink properties before, during and after 3D bioprinting. Biofabrication 2016;8(3); doi: 10.1088/1758-5090/8/3/032002.
119. Seyedmahmoud R, Çelebi-Saltik B, Barros N, et al. Three-dimensional bioprinting of functional skeletal muscle tissue using gelatin. Micromachines (Basel) 2019;10:1–12.
120. Gudapati H, Dey M, Ozbolat I. A comprehensive review on droplet-based bioprinting: Past, present and future. Biomaterials 2016;102:20–42; doi: 10.1016/j.biomaterials.2016.06.012.
121. Hinton TJ, Jallerat Q, Palchesko RN, et al. Three-dimensional printing of complex biological structures by freeform reversible embedding of suspended hydrogels. Sci Adv 2015;1(9); doi: 10.1126/sciadv.1500758.
122. Lee HJ, Koo YW, Yeo M, et al. Recent cell printing systems for tissue engineering. Int J Bioprint 2017;3(1):27–41; doi: 10.18063/IJB.2017.01.004.
123. Klekiel T, Mackiewicz A, Kaczmarek-Pawelska A, et al. Novel design of sodium alginate based absorbable stent for the use in urethral stricture disease. Journal of Materials Research and Technology 2020;9(4):9004–9015; doi: 10.1016/j.jmrt.2020.06.047.
124. Kurowiak J, Kaczmarek-Pawelska A, Mackiewicz AG, et al. Analysis of the degradation process of alginate-based hydrogels in artificial urine for use as a bioresorbable material in the treatment of urethral injuries. Processes 2020;8(3); doi: 10.3390/pr8030304.
125. Zhu K, Shin SR, van Kempen T, et al. Gold Nanocomposite Bioink for Printing 3D Cardiac Constructs. Adv Funct Mater 2017;27(12); doi: 10.1002/adfm.201605352.
126. Jia J, Richards DJ, Pollard S, et al. Engineering alginate as bioink for bioprinting. Acta Biomater 2014;10(10):4323–4331; doi: 10.1016/j.actbio.2014.06.034.
127. Cen L, Liu WEI, Cui LEI, et al. Collagen Tissue Engineering: Development of Novel Biomaterials and Applications. 2000;63(5):492–496.
128. Rodriguez-Pascual F, Slatter DA. Collagen cross-linking: Insights on the evolution of metazoan extracellular matrix. Sci Rep 2016;6(November):1–7; doi: 10.1038/srep37374.
129. Mori H, Shimizu K, Hara M. Dynamic viscoelastic properties of collagen gels with high mechanical strength. Materials Science and Engineering C 2013;33(6):3230–3236; doi: 10.1016/j.msec.2013.03.047.

130. Dong C, Lv Y. Application of collagen scaffold in tissue engineering: Recent advances and new perspectives. Polymers (Basel) 2016;8(2):1–20; doi: 10.3390/polym8020042.
131. Yang X, Lu Z, Wu H, et al. Collagen-alginate as bioink for three-dimensional (3D) cell printing based cartilage tissue engineering. Materials Science and Engineering C 2018;83(June 2017):195–201; doi: 10.1016/j.msec.2017.09.002.
132. Afewerki S, Sheikhi A, Kannan S, et al. Gelatin-polysaccharide composite scaffolds for 3D cell culture and tissue engineering: Towards natural therapeutics. Bioeng Transl Med 2019;4(1):96–115; doi: 10.1002/btm2.10124.
133. Mad-Ali S, Benjakul S, Prodpran T, et al. Characteristics and gelling properties of gelatin from goat skin as affected by drying methods. J Food Sci Technol 2017;54(6):1646–1654; doi: 10.1007/s13197-017-2597-5.
134. Bupphathong S, Quiroz C, Huang W, et al. Gelatin Methacrylate Hydrogel for Tissue Engineering Applications—A Review on Material Modifications. Pharmaceuticals 2022;15(2):1–27; doi: 10.3390/ph15020171.
135. Pelham RJ, Wang YL. Cell locomotion and focal adhesions are regulated by substrate flexibility. Proc Natl Acad Sci U S A 1997;94(25):13661–13665; doi: 10.1073/pnas.94.25.13661.
136. McDaniel DP, Shaw GA, Elliott JT, et al. The stiffness of collagen fibrils influences vascular smooth muscle cell phenotype. Biophys J 2007;92(5):1759–1769; doi: 10.1529/biophysj.106.089003.
137. Yi B, Shen Y, Tang H, et al. Stiffness of Aligned Fibers Regulates the Phenotypic Expression of Vascular Smooth Muscle Cells. ACS Appl Mater Interfaces 2019;11(7):6867–6880; doi: 10.1021/acsami.9b00293.
138. Ghazanfari S, Tafazzoli-Shadpour M, Shokrgozar MA. Effects of cyclic stretch on proliferation of mesenchymal stem cells and their differentiation to smooth muscle cells. Biochem Biophys Res Commun 2009;388(3):601–605; doi: 10.1016/j.bbrc.2009.08.072.
139. Huang H, Kamm RD, Lee RT. Cell mechanics and mechanotransduction: Pathways, probes, and physiology. Am J Physiol Cell Physiol 2004;287(1 56-1):1–11; doi: 10.1152/ajpcell.00559.2003.
140. Haberstroh KM, Kaefer M, Retik AB, et al. The effects of sustained hydrostatic pressure on select bladder smooth muscle cell functions. Journal of Urology 1999;162(6):2114–2118; doi: 10.1016/S0022-5347(05)68136-0.
141. Nguyen HT, Adam RM, Bride SH, et al. Cyclic stretch activates p38 SAPK2-, ErbB2-, and AT1-dependent signaling in bladder smooth muscle cells. Am J Physiol Cell Physiol 2000;279(4 48-4):1155–1167; doi: 10.1152/ajpcell.2000.279.4.c1155.
142. Chae S, Kim J, Yi HG, et al. 3D Bioprinting of an In Vitro Model of a Biomimetic Urinary Bladder with a Contract-Release System. Micromachines (Basel) 2022;13(2); doi: 10.3390/mi13020277.
143. Wang JHC, Thampatty BP. An introductory review of cell mechanobiology. Biomech Model Mechanobiol 2006;5(1):1–16; doi: 10.1007/s10237-005-0012-z.
144. Adam RM, Roth JA, Cheng HL, et al. Signaling through P13K/AKT mediates stretch and PDGF-BBdependent DNA synthesis in bladder smooth muscle cells. Journal of Urology 2003;169(6):2388–2393; doi: 10.1097/01.ju.0000063980.99368.35.
145. Hook SH, Lee HJ, Chung WT, et al. Cyclic mechanical stretch stimulates the proliferation of C2C12 myoblasts and inhibits their differentiation via prolonged activation of p38 MAPK. Mol Cells 2008;25(4):479–486.
146. Hosseini V, Ahadian S, Ostrovidov S, et al. Engineered contractile skeletal

muscle tissue on a microgrooved methacrylated gelatin substrate. Tissue Eng Part A 2012;18(23–24):2453–2465; doi: 10.1089/ten.tea.2012.0181.
147. Colosi C, Shin SR, Manoharan V, et al. Microfluidic Bioprinting of Heterogeneous 3D Tissue Constructs Using Low-Viscosity Bioink. Advanced Materials 2016;28(4):677–684a; doi: 10.1002/adma.201503310.
148. Yin J, Yan M, Wang Y, et al. 3D Bioprinting of Low-Concentration Cell-Laden Gelatin Methacrylate (GelMA) Bioinks with a Two-Step Cross-linking Strategy. ACS Appl Mater Interfaces 2018;10(8):6849–6857; doi: 10.1021/acsami.7b16059.
149. Levato R. Biofabrication of tissue constructs by 3D bioprinting of cell-laden microcarriers. Biofabrication 2014;6(3):035020.
150. Bupphathong S, Quiroz C, Huang W, et al. Gelatin Methacrylate Hydrogel for Tissue Engineering Applications—A Review on Material Modifications. Pharmaceuticals 2022;15(2); doi: 10.3390/ph15020171.
151. Stoppel WL, White JC, Horava SD, et al. Terminal sterilization of alginate hydrogels: Efficacy and impact on mechanical properties. J Biomed Mater Res B Appl Biomater 2014;102(4):877–884; doi: 10.1002/jbm.b.33070.
152. Nguyen AK, Goering PL, Reipa V, et al. Toxicity and photosensitizing assessment of gelatin methacryloyl-based hydrogels photoinitiated with lithium phenyl-2,4,6-trimethylbenzoylphosphinate in human primary renal proximal tubule epithelial cells. Biointerphases 2019;14(2):021007; doi: 10.1116/1.5095886.
153. Du W, Chen J, Li H, et al. Direct cellular organization with ring-shaped composite polymers and glass substrates for urethral sphincter tissue engineering. J Mater Chem B 2016;4(22):3998–4008; doi: 10.1039/c6tb00437g.
154. Makamba H, Kim JH, Lim K, et al. Surface modification of poly(dimethylsiloxane) microchannels. Electrophoresis 2003;24(21):3607–3619; doi: 10.1002/elps.200305627.
155. Cha C, Antoniadou E, Lee M, et al. Tailoring hydrogel adhesion to polydimethylsiloxane substrates using polysaccharide glue. Angewandte Chemie - International Edition 2013;52(27):6949–6952; doi: 10.1002/anie.201302925.
156. Wazir R, Luo DY, Tian Y, et al. The purinergic component of human bladder smooth muscle cells' proliferation and contraction under physiological stretch. Biochem Biophys Res Commun 2013;437(2):256–260; doi: 10.1016/j.bbrc.2013.06.059.
157. Wang F, Zachar V, Pennisi CP, et al. Hypoxia enhances differentiation of adipose tissue-derived stem cells toward the smooth muscle phenotype. Int J Mol Sci 2018;19(2); doi: 10.3390/ijms19020517.
158. Malda J, Visser J, Melchels FP, et al. 25th anniversary article: Engineering hydrogels for biofabrication. Advanced Materials 2013;25(36):5011–5028; doi: 10.1002/adma.201302042.
159. Ji S, Guvendiren M. Recent Advances in Bioink Design for 3D Bioprinting of Tissues and Organs. Front Bioeng Biotechnol 2017;5(APR):1–8; doi: 10.3389/fbioe.2017.00023.
160. Ying G, Jiang N, Yu C, et al. Three-dimensional bioprinting of gelatin methacryloyl (GelMA). Biodes Manuf 2018;1(4):215–224; doi: 10.1007/s42242-018-0028-8.
161. Yue K, Trujillo-de Santiago G, Alvarez MM, et al. Synthesis, properties, and biomedical applications of gelatin methacryloyl (GelMA) hydrogels. Biomaterials 2015;73:254–271; doi: 10.1016/j.biomaterials.2015.08.045.
162. Aldana AA, Valente F, Dilley R, et al. Development of 3D bioprinted GelMA-

alginate hydrogels with tunable mechanical properties. Bioprinting 2021;21(June 2020):e00105; doi: 10.1016/j.bprint.2020.e00105.
163. Sears NA, Seshadri DR, Dhavalikar PS, et al. A Review of Three-Dimensional Printing in Tissue Engineering. Tissue Eng Part B Rev 2016;22(4):298–310; doi: 10.1089/ten.teb.2015.0464.
164. Lawrence KP, Douki T, Sarkany RPE, et al. The UV/Visible Radiation Boundary Region (385–405 nm) Damages Skin Cells and Induces "dark" Cyclobutane Pyrimidine Dimers in Human Skin in vivo. Sci Rep 2018;8(1):1–12; doi: 10.1038/s41598-018-30738-6.
165. Wong DY, Ranganath T, Kasko AM. Low-dose, long-wave UV light does not affect gene expression of human mesenchymal stem cells. PLoS One 2015;10(9):1–21; doi: 10.1371/journal.pone.0139307.
166. Junbin Shi, 1, 2, 3 Malcolm M. Q. Xing, 2, 3, 4,* and Wen Zhong1 5. Development of Hydrogels and Biomimetic Regulators as Tissue Engineering Scaffolds. Membranes (Basel) 2012;2:70–90.
167. Sazonova O v., Isenberg BC, Herrmann J, et al. Extracellular matrix presentation modulates vascular smooth muscle cell mechanotransduction. Matrix Biology 2015;41:36–43; doi: 10.1016/j.matbio.2014.11.001.
168. Lin H, Qiu X, Du Q, et al. Engineered Microenvironment for Manufacturing Human Pluripotent Stem Cell-Derived Vascular Smooth Muscle Cells. Stem Cell Reports 2019;12(1):84–97; doi: 10.1016/j.stemcr.2018.11.009.
169. Brandl F, Sommer F, Goepferich A. Rational design of hydrogels for tissue engineering: Impact of physical factors on cell behavior. Biomaterials 2007;28(2):134–146; doi: 10.1016/j.biomaterials.2006.09.017.
170. Jensen LF, Bentzon JF, Albarrán-juárez J. The phenotypic responses of vascular smooth muscle cells exposed to mechanical cues. Cells 2021;10(9):1–20; doi: 10.3390/cells10092209.
171. Vaes RDW, van den Berk L, Boonen B, et al. A novel human cell culture model to study visceral smooth muscle phenotypic modulation in health and disease. Am J Physiol Cell Physiol 2018;315(4):C598–C607; doi: 10.1152/ajpcell.00167.2017.
172. Kindy MS, Chang CJ, Sonenshein GE. Serum deprivation of vascular smooth muscle cells enhances collagen gene expression. Journal of Biological Chemistry 1988;263(23):11426–11430; doi: 10.1016/s0021-9258(18)37974-2.
173. Engler AJ, Sen S, Sweeney HL, et al. Matrix Elasticity Directs Stem Cell Lineage Specification. Cell 2006;126(4):677–689; doi: 10.1016/j.cell.2006.06.044.
174. Jensen C, Gurevich L, Patriciu A, et al. Increased connective tissue attachment to silicone implants by a water vapor plasma treatment. J Biomed Mater Res A 2012;100 A(12):3400–3407; doi: 10.1002/jbm.a.34284.
175. Camci-Unal G, Cuttica D, Annabi N, et al. Synthesis and characterization of hybrid hyaluronic acid-gelatin hydrogels. Biomacromolecules 2013;14(4):1085–1092; doi: 10.1021/bm3019856.
176. Bovone G, Dudaryeva OY, Marco-Dufort B, et al. Engineering Hydrogel Adhesion for Biomedical Applications via Chemical Design of the Junction. ACS Biomater Sci Eng 2021;7(9):4048–4076; doi: 10.1021/acsbiomaterials.0c01677.
177. Bakry R, Bonn GK, Mair D, et al. Monolithic porous polymer layer for the separation of peptides and proteins using thin-layer chromatography coupled with MALDI-TOF-MS. Anal Chem 2007;79(2):486–493; doi: 10.1021/ac061527i.

178. Zheng B, Liu Y, Li D, et al. Hydrophobic-hydrophilic monolithic dual-phase layer for two-dimensional thin-layer chromatography coupled with surface-enhanced Raman spectroscopy detection. J Sep Sci 2015;38(15):2737–2745; doi: 10.1002/jssc.201500243.
179. Slabospitskaya MY, Vlakh EG, Saprykina NN, et al. Synthesis and investigation of a new macroporous monolithic material based on an N-hydroxyphthalimide ester of acrylic acid-co-glycidyl methacrylate-co-ethylene dimethacrylate terpolymer. J Appl Polym Sci 2009;111(2):692–700; doi: 10.1002/app.29130.
180. Pennisi CP, Olesen CG, de Zee M, et al. Uniaxial cyclic strain drives assembly and differentiation of skeletal myocytes. Tissue Eng Part A 2011;17(19–20):2543–2550; doi: 10.1089/ten.tea.2011.0089.
181. Levesque L, Mantovani D. The effect of dynamical strain on the maturation of collagen-based cell-containing scaffolds for vascular tissue engineering. Adv Mat Res 2012;409:152–157; doi: 10.4028/www.scientific.net/AMR.409.152.
182. Jokandan MS, Ajalloueian F, Edinger M, et al. Bladder wall biomechanics: A comprehensive study on fresh porcine urinary bladder. J Mech Behav Biomed Mater 2018;79(July 2017):92–103; doi: 10.1016/j.jmbbm.2017.11.034.
183. Bono N, Pezzoli D, Levesque L, et al. Unraveling the role of mechanical stimulation on smooth muscle cells: A comparative study between 2D and 3D models. Biotechnol Bioeng 2016;113(10):2254–2263; doi: 10.1002/bit.25979.
184. Asano S, Ito S, Morosawa M, et al. Cyclic stretch enhances reorientation and differentiation of 3-D culture model of human airway smooth muscle. Biochem Biophys Rep 2018;16(July):32–38; doi: 10.1016/j.bbrep.2018.09.003.
185. Kim BS, Nikolovski J, Bonadio J, et al. Cyclic mechanical strain regulates the development of engineered smooth muscle tissue. Nat Biotechnol 1999;17(10):979–983; doi: 10.1038/13671.
186. Hornberger TA, Armstrong DD, Koh TJ, et al. Intracellular signaling specificity in response to uniaxial vs. multiaxial stretch: Implications for mechanotransduction. Am J Physiol Cell Physiol 2005;288(1 57-1):185–195; doi: 10.1152/ajpcell.00207.2004.
187. Adam RM. Recent insights into the cell biology of bladder smooth muscle. Nephron Exp Nephrol 2006;102(1):1–8; doi: 10.1159/000088310.
188. Chaudhuri S, Smith PG. Cyclic strain-induced HSP27 phosphorylation modulates actin filaments in airway smooth muscle cells. Am J Respir Cell Mol Biol 2008;39(3):270–278; doi: 10.1165/rcmb.2007-0263OC.
189. Wazir R, Luo DY, Dai Y, et al. Expression and proliferation profiles of PKC, JNK and p38MAPK in physiologically stretched human bladder smooth muscle cells. Biochem Biophys Res Commun 2013;438(3):479–482; doi: 10.1016/j.bbrc.2013.07.115.

APPENDICES: PAPER I-III

ISSN (online): 2246-1302
ISBN (online): 978-87-7573-822-9

AALBORG UNIVERSITY PRESS